Metabolic Engineering 41 (2017) 67–81

Contents lists available at ScienceDirect

Metabolic Engineering

journal homepage: www.elsevier.com/locate/ymben

Original Research Article

An integrated network analysis reveals that nitric oxide reductase prevents metabolic cycling of nitric oxide by *Pseudomonas aeruginosa*

Jonathan L. Robinson[a,1], Jacob M. Jaslove[b,c], Allison M. Murawski[b,c], Christopher H. Fazen[a,2], Mark P. Brynildsen[a,b,*]

[a] *Department of Chemical and Biological Engineering, Princeton University, Princeton, NJ 08544, USA*
[b] *Department of Molecular Biology, Princeton University, Princeton, NJ 08544, USA*
[c] *Rutgers Robert Wood Johnson Medical School, Piscataway, NJ 08854, USA*

ARTICLE INFO

Keywords:
Metabolic cycle
Kinetic model
Oscillations
NO reductase
Fhp
Denitrification

ABSTRACT

Nitric oxide (NO) is a chemical weapon within the arsenal of immune cells, but is also generated endogenously by different bacteria. *Pseudomonas aeruginosa* are pathogens that contain an NO-generating nitrite (NO_2^-) reductase (NirS), and NO has been shown to influence their virulence. Interestingly, *P. aeruginosa* also contain NO dioxygenase (Fhp) and nitrate (NO_3^-) reductases, which together with NirS provide the potential for NO to be metabolically cycled ($NO \rightarrow NO_3^- \rightarrow NO_2^- \rightarrow NO$). Deeper understanding of NO metabolism in *P. aeruginosa* will increase knowledge of its pathogenesis, and computational models have proven to be useful tools for the quantitative dissection of NO biochemical networks. Here we developed such a model for *P. aeruginosa* and confirmed its predictive accuracy with measurements of NO, O_2, NO_2^-, and NO_3^- in mutant cultures devoid of Fhp or NorCB (NO reductase) activity. Using the model, we assessed whether NO was metabolically cycled in aerobic *P. aeruginosa* cultures. Calculated fluxes indicated a bottleneck at NO_3^-, which was relieved upon O_2 depletion. As cell growth depleted dissolved O_2 levels, NO_3^- was converted to NO_2^- at near-stoichiometric levels, whereas NO_2^- consumption did not coincide with NO or NO_3^- accumulation. Assimilatory NO_2^- reductase (NirBD) or NorCB activity could have prevented NO cycling, and experiments with Δ*nirB*, Δ*nirS*, and Δ*norC* showed that NorCB was responsible for loss of flux from the cycle. Collectively, this work provides a computational tool to analyze NO metabolism in *P. aeruginosa*, and establishes that *P. aeruginosa* use NorCB to prevent metabolic cycling of NO.

1. Introduction

Pseudomonas aeruginosa are a common cause of infections on biomedical devices, at surgical sites, and within the airways of cystic fibrosis patients (Driscoll et al., 2007; Winstanley et al., 2016). Treatment of *P. aeruginosa* infections is difficult because they are Gram-negative bacteria that are avid biofilm formers (O'Toole and Kolter, 1998; Drenkard and Ausubel, 2002) and they possess both broad-spectrum β-lactamases and numerous multidrug efflux pumps, which make them naturally resistant to many antibiotics (Breidenstein et al., 2011; Gellatly and Hancock, 2013). Further, antibiotics that were once effective against *P. aeruginosa*, such as fluoroquinolones and aminoglycosides, are now innocuous to many clinical isolates due to the rise and spread of multidrug resistant (MDR) strains (Poole, 2011). This confluence of challenges has motivated many searches for new agents or methodologies to treat *P. aeruginosa* infections (Siryaporn et al., 2014; Ketelboeter et al., 2014; Miller et al., 2015; Hentzer et al., 2003). One particularly promising avenue involves targeting the processes that pathogens use to cause illness rather than those that are essential to its propagation under any circumstance (Hentzer et al., 2003). Conventional antibiotics fall into the latter category, applying selective pressure both inside and outside the human body (*e.g.*, sewage, soil, water), whereas antivirulence therapies comprise the former category, confining selective pressure to within the host (Allen et al., 2014; Cegelski et al., 2008; Escaich, 2008; Baquero et al., 2008). Such agents would be orthogonal to current treatments, and their focused nature is projected to produce resistance at far greater time scales than antibiotics (Allen et al., 2014).

* Correspondence to: School of Engineering and Applied Science, Department of Chemical and Biological Engineering, Princeton University, 205 Hoyt Laboratory, 25 William Street, Princeton, NJ 08544, USA.
E-mail address: mbrynild@princeton.edu (M.P. Brynildsen).
[1] Present address: Department of Biology and Biological Engineering, Chalmers University of Technology, SE412 96 Gothenburg, Sweden.
[2] Present address: Department of Chemistry, The College of New Jersey, Ewing, NJ 08628, USA.

http://dx.doi.org/10.1016/j.ymben.2017.03.006
Received 25 July 2016; Received in revised form 21 December 2016; Accepted 27 March 2017
Available online 29 March 2017

To facilitate the development of antivirulence therapies, much work has been conducted to increase understanding of *P. aeruginosa* pathogenesis and its physiology within host environments (Gellatly and Hancock, 2013; Hauser, 2009; O'Loughlin et al., 2013; Yoon et al., 2002). During pathogenesis, *P. aeruginosa* are exposed to nitric oxide (NO) generated by immune cells, such as macrophages (Darling and Evans, 2003; Kakishima et al., 2007). NO is a toxic metabolite that readily reacts with iron-sulfur clusters ([Fe-S]), heme cofactors, and other transition metal centers, and several of its autoxidation products can damage free or protein-bound thiols, tyrosine residues, and DNA bases (Bowman et al., 2011; Hyduke et al., 2007; Poole and Hughes, 2000; Robinson et al., 2014a). To counteract the nitrosative assault of immune cells, *P. aeruginosa* employ detoxification systems, such NO reductase and NO dioxygenase, which are encoded by *norCB* and *fhp*, respectively (Arai et al., 2005, 1995). In essence, *P. aeruginosa* employs these enzymes to divert flux of NO away from reactions that damage the pathogen (*e.g.*, nitrosylation of Fe-S clusters) toward reactions that neutralize this toxic metabolite (*e.g.*, reduction to N_2O). From a metabolic engineering perspective, this is analogous to a biocatalyst (*P. aeruginosa*) that has metabolic pathways (NO detoxification) that divert substrate (NO) away from the desired pathway (damage to biomolecules), and thus reduce product yield (killing of *P. aeruginosa*) (Chou and Brynildsen, 2016). A strategy to improve desirable outcomes would be to eliminate competing pathways, and Kakishima and colleagues have shown this with *P. aeruginosa* and NO detoxification where *P. aeruginosa* devoid of NorCB were killed more quickly than wild-type (WT) by LPS-activated macrophages, and that the survival difference was eliminated with use of an inducible nitric oxide synthase (iNOS) inhibitor (Kakishima et al., 2007).

Beyond improving survival in macrophages, *P. aeruginosa* NO metabolism has been associated with numerous pathogenic processes (Barraud et al., 2006, 2009; Van Alst et al., 2009a, 2007). For example, NO was found to stimulate dispersal of *P. aeruginosa* biofilms by increasing phosphodiesterase activity, which reduced the level of cyclic-di-GMP (Barraud et al., 2009). Endogenous NO production by *P. aeruginosa* from one of its NO_2^- reductases (NirS) has been identified as a mediator of both virulence factor expression and biofilm dispersal (Barraud et al., 2006; Van Alst et al., 2007). Van Alst and colleagues observed that both Δ*narGH* and Δ*nirS P. aeruginosa* were far less virulent to *Caenorhabditis elegans* than the WT (Van Alst et al., 2007). In a later study, the same mutants were shown to be more sensitive to killing by human monocytes, and found to be defective in expression of a type III secretion system (Van Alst et al., 2009a). Barraud and colleagues observed that biofilms of Δ*nirS* dispersed far less than those of WT, and provided evidence that low concentrations of NO were the cause (Barraud et al., 2006). Importantly, NO_2^- is a relatively stable end product of the reaction of NO with O_2, and can therefore be present at infection sites (Hassett et al., 2002).

The influence of the *P. aeruginosa* NO network on pathogenic processes suggests that deeper quantitative understanding of how it functions as a system could reveal strategies to sabotage *P. aeruginosa* pathogenesis. In this regard, a parallel can be drawn to metabolic engineering, where deeper knowledge of how metabolism functions as an interconnected system will reveal ways to improve chemical production. Such knowledge is provided with the use of computational models (Chowdhury et al., 2014; Karr et al., 2012; Khodayari et al., 2014), and the same applies to NO, which is a highly reactive molecule with an expansive biochemical reaction network (Robinson et al., 2014a; Robinson and Brynildsen, 2013; Lancaster, 2006; Lim et al., 2008). Computational models of NO biochemistry and regulation have increased understanding of NO biology from mammalian to bacterial systems (Robinson and Brynildsen, 2013; Lancaster, 2006; Lim et al., 2008; Bagci et al., 2008; Hu et al., 2006; Lewis et al., 1995; Robinson et al., 2014b), and in one recent example, we used a model of *E. coli* NO stress to unravel the mechanism behind NO oscillations in low O_2 environments (Robinson and Brynildsen, 2016a). With respect to *P. aeruginosa* and NO, a previous mathematical model of the regulatory network associated with denitrification was developed by Arat et al. (2015). In that study, a qualitative, discrete-variable model of the *P. aeruginosa* denitrification regulatory network was constructed to understand the impact of environmental variables, such as phosphate and O_2, on the system (Arat et al., 2015). Notably, that model was time-independent, encompassed only the denitrification pathway (NO_3^- to N_2), and was qualitative in the sense that all variables were either Boolean or ternary ("low", "medium", "high"). In addition, a genome-scale metabolic model of *P. aeruginosa* has been constructed (Oberhardt et al., 2008, 2011), which provides a valuable resource and framework for studies of the *P. aeruginosa* metabolic network (Oberhardt et al., 2010; Varga et al., 2015); however, the absence of kinetics and many NO-specific reactions precludes its use for dynamic analyses of NO stress in *P. aeruginosa*.

In this work, we had two goals: (1) develop a quantitative model of the *P. aeruginosa* NO network that would provide a computational tool for examination of the dynamics of this metabolic system, and (2) assess whether an NO cycle present in the metabolic network was functional (Fig. 1). Specifically, *P. aeruginosa* contains enzymes that can perform the conversion of $NO \rightarrow NO_3^- \rightarrow NO_2^- \rightarrow NO$. This cycle is composed of NO dioxygenase, NO_3^- reductase, and NO_2^- reductase activities, which would collectively deactivate NO, only to regenerate it in a subsequent enzymatic step. Interestingly, elevated levels of NO_2^- and NO_3^- have been found in the lungs of cystic fibrosis patients, who often suffer from *P. aeruginosa* infections, and this has been interpreted as an indication of increased NO production by host immune cells, which suggests that *P. aeruginosa* infection environments contain all three metabolites of the NO cycle (Hassett et al., 2002; Kolpen et al., 2014). In addition, the *P. aeruginosa* NO cycle network architecture is distinct from that of *Escherichia coli*, which has served as a model Gram-negative bacterium for the study of NO metabolism (Bowman et al., 2011; Robinson and Brynildsen, 2013; Mason et al.,

A

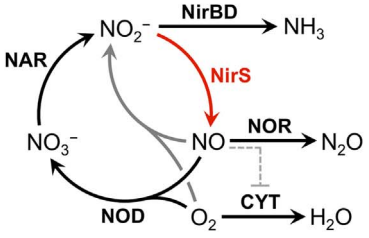

B

Function	Enzyme	Reaction
NOD	Fhp	$2\ NO + 2\ O_2 + NADH \rightarrow 2\ NO_3^- + NAD^+ + H^+$
NAR	NarGHI	*cytoplasm*: $NO_3^- + Q_8H_2 \rightarrow NO_2^- + Q_8 + H_2O$
	NapAB	*periplasm*: $NO_3^- + Q_8H_2 \rightarrow NO_2^- + Q_8 + H_2O$
NIR	NirBD	$NO_2^- + 3\ NADH + 4\ H^+ \rightarrow NH_3 + 3\ NAD^+ + 2\ H_2O$
	NirS	$NO_2^- + cytc_{Fe^{2+}} + 2\ H^+ \rightarrow NO + cytc_{Fe^{3+}} + H_2O$
NOR	NorCB	$2\ NO + Q_8H_2 \rightarrow N_2O + H_2O + Q_8$

Fig. 1. NO metabolic cycle subnetwork. (A) Simplified reaction network diagram illustrating the $NO \rightarrow NO_3^- \rightarrow NO_2^- \rightarrow NO$ metabolic cycle present in *P. aeruginosa*. Relevant reactions that remove flux from the cycle (catalyzed by NirBD and NOR) are also shown, as well as the NO-inhibited respiratory cytochromes (CYT) that compete with NOD for available O_2. Enzymes are in bold, near the reaction they catalyze. The autoxidation of NO by O_2 (gray arrow) is spontaneous, and thus has no associated enzyme. The network is comparable to that of *E. coli*, except *E. coli* lack an NO-generating NO_2^- reductase (shown in red), thus preventing the metabolic cycling of NO. For illustrative purposes, the reactions were not balanced in element or charge; thus, the table in (B) provides the balanced chemical equations. Q_8H_2 is ubiquinol; Q_8 is ubiquinone; $cytc_{Fe2+}$ and $cytc_{Fe3+}$ are the ferrous and ferric forms of cytochrome *c*, respectively. (For interpretation of the references to color in this figure legend, the reader is referred to the web version of this article).

2009; Gardner et al., 1998), because the NO_2^- reductases of *E. coli* generate ammonia (NH_3) rather than NO (Keseler et al., 2013; Cole, 1996), and thus *E. coli* does not have the capacity to cycle NO. In fact, *P. aeruginosa* has a similar, additional NO_2^- reductase (NirBD) that produces NH_3, which would prevent an NO cycle, as well as an NO reductase (NorCB) that would convert NO to N_2O (Arai et al., 1995; Romeo et al., 2012; Winsor et al., 2016). Due to these potential exit strategies and differences that exist in the regulation of these enzymes (Romeo et al., 2012; Kuroki et al., 2014), it was uncertain whether an NO cycle would occur.

To accomplish the first of our goals, we constructed a quantitative, kinetic model of NO stress in *P. aeruginosa*, and experimentally validated its predictions of NO metabolism in mutants devoid of NO dioxygenase and NO reductase, Δ*fhp* and Δ*norC*, respectively. This model can serve as a valuable tool to calculate fluxes of NO through cellular and non-cellular pathways in *P. aeruginosa* cultures, which is an important task for any metabolic system where competition for substrate limits desirable outcomes. Using this model, we calculated fluxes through NO dioxygenase, NO_3^- reductase, and NO_2^- reductase during and immediately following NO stress, which suggested that NO_3^- reductase was not functioning appreciably. Given the role of O_2 in regulation of NO_3^- reductase activity (Hernandez and Rowe, 1987; Schreiber et al., 2007), we allowed cultures to grow and deplete O_2 from the media. When dissolved O_2 concentrations dropped to ~3 μM, NO_3^- consumption and NO_2^- accumulation were observed. Interestingly, NO became briefly detectable upon NO_2^- accumulation, but the quantitative amounts were small and NO_3^- failed to accumulate again, which pointed to a mechanism by which *P. aeruginosa* prevented the NO cycle. Subsequent analyses with genetic mutants identified NO reductase (NorCB) as the major enzyme removing flux from the NO cycle, and in its absence, NO concentrations oscillated with an amplitude (defined here as the peak NO concentration) of ~3 μM and period of ~3 min. These oscillations were consistent with a recently identified stress-metabolic oscillator that originates from a competition for O_2 between NO dioxygenase and aerobic respiratory terminal oxidases (Robinson and Brynildsen, 2016a). Given the difference in oscillation dynamics from those observed previously, we evaluated the impact of varying key model parameters on oscillation behavior. The analysis revealed that the oscillation period and amplitude are sensitive to many changes in species and culturing conditions, and identified NO-mediated substrate inhibition of NO dioxygenase as a necessary feature for oscillations. Finally, to provide additional experimental support for the NO cycling mechanism and the associated role of NorCB, we demonstrated that the NO cycle can be initiated by the addition of NO_3^- to Δ*norC* cultures, but that it is not appreciably active when NorC is present. Collectively, this study provides a computational tool to quantitatively analyze NO fluxes through desired and competing reactions in *P. aeruginosa* cultures, and demonstrates that NorCB prevents cycling of NO in *P. aeruginosa* cultures.

2. Results

2.1. Construction of a quantitative kinetic model of NO metabolism in P. aeruginosa

2.1.1. Model construction

A quantitative kinetic model of the NO stress network in *P. aeruginosa* PAO1 was constructed using an existing *E. coli* K-12 MG1655 model (Robinson and Brynildsen, 2016a) as a template, and following a procedure that was recently implemented to develop a model for enterohemorrhagic *E. coli* O157:H7 (Robinson and Brynildsen, 2016b) (see Section 4.7 for additional construction details, Table S1 for model species, Tables S2 and S3 for model reactions, and Model S1 for the complete model file). A large amount of the *E. coli* model structure was retained, including 113 biochemical species (77% of the *E. coli* model), 119 reaction rate expressions (69%), and 131 kinetic parameters (69%), but there were also a number of substantial changes needed to adapt the model to *P. aeruginosa*. The most notable differences between the *E. coli* and *P. aeruginosa* networks involved the aerobic respiratory quinol oxidases and the denitrification enzymes. *E. coli* possesses three aerobic (O_2-consuming) cytochrome quinol oxidases: cytochromes *bo*, *bd*-I, and *bd*-II (Cyo, Cyd, and AppCB, respectively) (Keseler et al., 2013). *P. aeruginosa*, however, harbors five different cytochrome terminal oxidases, two of which are ubiquinol oxidases (Cyo and cyanide insensitive oxidase (CIO)), whereas the other three are cytochrome *c* oxidases (Cbb3-1, Cbb3-2, and Aa3) (Arai, 2011; Kanehisa et al., 2016). The three *E. coli* quinol oxidases in the model were therefore replaced with the five *P. aeruginosa* systems.

The NO, NO_2^-, and NO_3^- processing pathways share some similarities between *E. coli* and *P. aeruginosa*; specifically, NO dioxygenase (Hmp in *E. coli*, Fhp in *P. aeruginosa*), and NO, NO_2^-, and NO_3^- reductases (NOR, NIR, and NAR, respectively) are present in both species. However, *P. aeruginosa* possesses an additional type of NIR that reduces NO_2^- to generate NO (dissimilatory NIR, NirS) in addition to a NIR that generates NH_3 (assimilatory NIR, NirBD). This is of particular interest because NirS would enable NO to be generated endogenously from NO_2^- (Fig. 1), which is a function that has been shown previously to modulate biofilm dispersal and expression of virulence factors in *P. aeruginosa* (Barraud et al., 2006, 2009). Therefore, the NIR and NAR enzymes of *P. aeruginosa* were added to the model. Furthermore, the transcriptional regulatory network governing expression of these and the NO detoxification enzymes was reconstructed in the PAO1 model to account for differences in regulatory structure from that of *E. coli*. This involved the addition of three transcription factors to the PAO1 model: the anaerobic response regulator (ANR), denitrification response regulator (DNR), and a two-component NO_3^- sensing regulator (NarXL) (Section 4.7 and Fig. S1) (Arai, 2011). These three transcription factors and their regulatory interactions were also included in the *P. aeruginosa* regulatory network constructed by Arat et al. (2015); however, the present implementation enables quantitative analysis of time-dependent changes in this pathway, and does so in the context of a larger, more expansive network.

2.1.2. Model training

After model construction was completed, the uncertain or unavailable parameters were trained on experimental measurements. The extracellular (organism-independent) parameters governing processes specific to the experimental apparatus were optimized first, and those were the rate of NO exchange with the gas phase, dissociation rate of DPTA NONOate to release NO, and the rate of spontaneous NO autoxidation in the media (Table S4). The parameters were optimized to simultaneously minimize error (sum of the squared residuals, SSR) between simulated and experimentally measured NO, NO_2^-, and NO_3^- concentrations following treatment of cell-free growth media with 50 μM DPTA (Section 4.8.1). Although the [NO] was measured continuously (> 1 read/s), only the data points corresponding to the 5 times at which [NO_2^-] and [NO_3^-] were measured (0, 0.5, 1.0, 1.5, and 2.0 h post-DPTA dose) were used, to avoid unevenly weighting the optimization toward [NO] data. Once the optimized parameter values were obtained, a subsequent MCMC procedure was performed whereby a random walk through parameter space was conducted to identify additional sets of parameter values that were sufficiently similar in agreement with the data (evidence ratio, ER < 10), yielding an ensemble of viable models (Section 4.8.2) (Robinson and Brynildsen, 2016a; Adolfsen and Brynildsen, 2015). The resulting [NO], [NO_2^-], and [NO_3^-] curves simulated by the ensemble were in excellent agreement with experimental measurements (Fig. S2).

Optimization of cellular parameters was performed in modules to improve computational feasibility by reducing the available solution space (Section 4.8.3). The respiratory module was trained first, where parameters governing aerobic respiration, 27 in total, were optimized

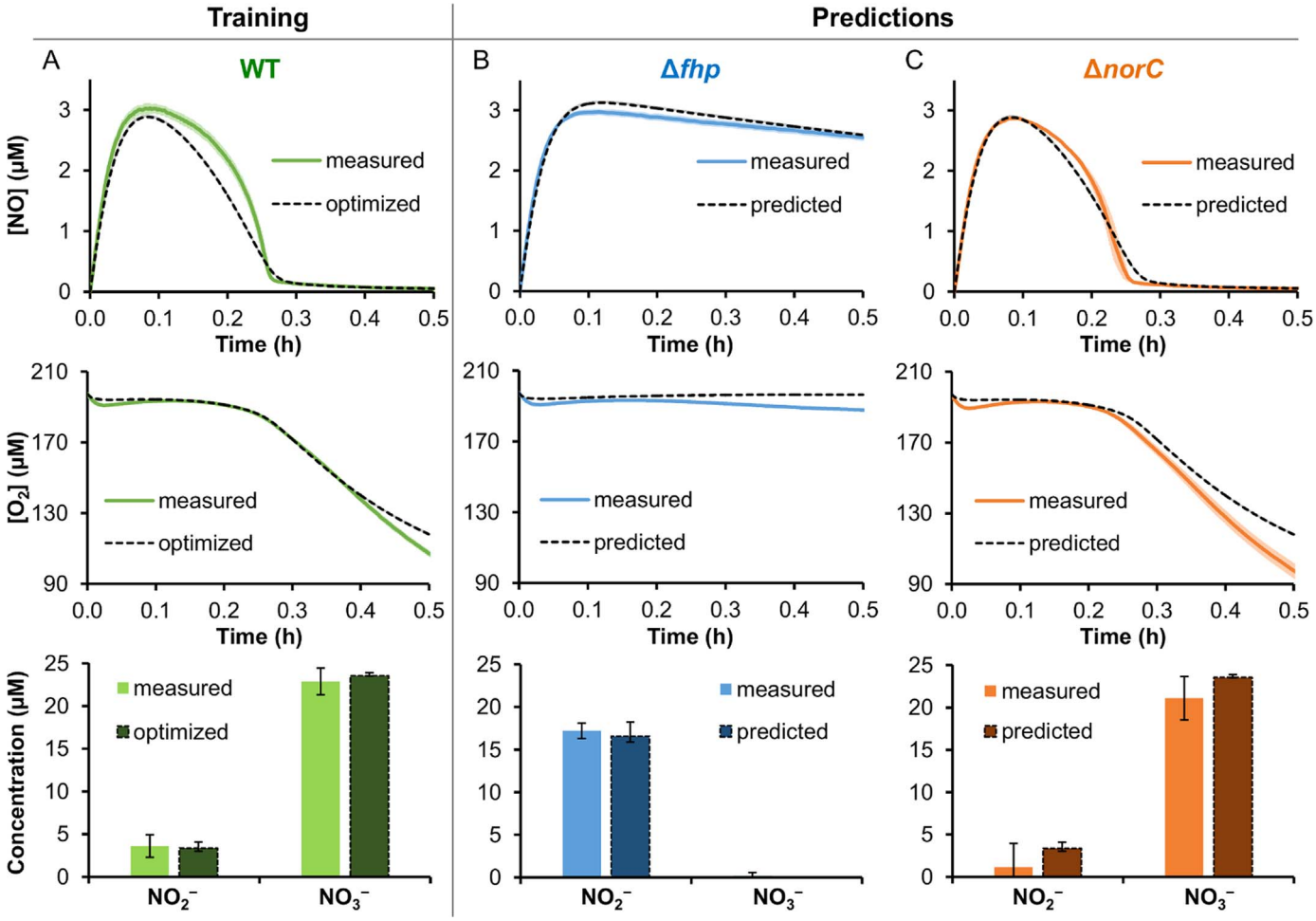

Fig. 2. Model training and experimental validation. (A) The model was trained on continuous measurements of [NO] and [O_2], and a single measurement at 0.5 h of [NO_2^-] and [NO_3^-] in aerobic wild-type PAO1 cultures at an initial OD_{600} of 0.05, treated with 50 μM DPTA at time zero. The ensemble of viable models was used to predict [NO], [O_2], [NO_2^-], and [NO_3^-] in cultures of PAO1 mutants (B) Δ*fhp* and (C) Δ*norC*, and the corresponding experiments were conducted and are shown. All measurements (solid lines or columns) are the mean of 3 independent experiments, with light shading (or error bars) representing the standard error of the mean (SEM). Dashed lines (or dashed-border columns) are simulation results obtained using the best-fit optimized parameter set, with gray shading (or error bars) representing parametric variation among the ensemble of viable (ER < 10) models.

to fit [O_2] data measured in untreated PAO1 cultures (Table S5). The optimization process mirrored that described for the extracellular parameters, where a subsequent MCMC procedure was performed to allow estimation of parameter and prediction uncertainty. The simulated [O_2] curve generated using the ensemble of models exhibited excellent agreement with experimental measurements (Fig. S3).

The final model training process involved all the remaining cellular parameters governing NO-stress related damage, inhibition, detoxification, and repair. A total of 137 parameters were optimized to simultaneously fit [NO] and [O_2] curves, as well as [NO_2^-] and [NO_3^-] at 0.5 h post-DPTA treatment, measured in a WT culture of *P. aeruginosa* treated with 50 μM DPTA (Table S6). To incorporate uncertainty of cell-free and respiratory parameter values into the final ensemble of models, those parameters were included with the other 137 cellular parameters in the subsequent MCMC analysis and permitted to vary within their confidence intervals (CIs), which were determined in the above-mentioned steps (Section 4.8.3). Simulations run using the resulting ensemble were in good agreement with measured [NO], [O_2], [NO_2^-], and [NO_3^-] data (Fig. 2A).

2.1.3. Experimental validation of model predictions

The predictive accuracy of the model was assessed by comparing simulated and measured [NO], [O_2], [NO_2^-], and [NO_3^-] data for cultures of *P. aeruginosa* mutants lacking either of the two major NO detoxification systems: NO dioxygenase (Δ*fhp*) and NO reductase (Δ*norC*). Simulations predicted negligible differences in NO, O_2, NO_2^-, and NO_3^- concentrations between WT and Δ*norC* cultures, whereas the Δ*fhp* mutant was predicted to exhibit severe inhibition of NO detoxification and, as a result, respiration. The greater importance of Fhp compared to NorCB under these conditions was expected, given that NO dioxygenases have been shown to dominate NO detoxification under aerobic conditions, whereas anaerobic conditions are favorable for NO reductase activity (Arai et al., 2005, 1995; Robinson and Brynildsen, 2013, 2016a; Zumft, 1997; Gardner, 2005). The corresponding experiments were performed, for which cultures of Δ*fhp* and Δ*norC* were treated with 50 μM DPTA NONOate under aerobic conditions. The predicted and measured [NO] and [O_2] curves, as well as [NO_2^-] and [NO_3^-] at 0.5 h post-dose were in excellent agreement for both mutants, demonstrating that the model had correctly predicted the contributions of Fhp and NorCB to aerobic NO detoxification (Fig. 2B and C, respectively).

2.2. Computational analysis of NO cycle activity

An interesting difference between the NO biochemical reaction networks of *E. coli* and *P. aeruginosa* is the presence of a NO-generating NO_2^- reductase in *P. aeruginosa* (NirS). With NirS, *P. aeruginosa* could conceivably detoxify NO with Fhp to form NO_3^-, the NO_3^- could be processed by NAR to generate NO_2^-, and NirS could generate NO from the resulting NO_2^- (Fig. 1). This three-enzyme

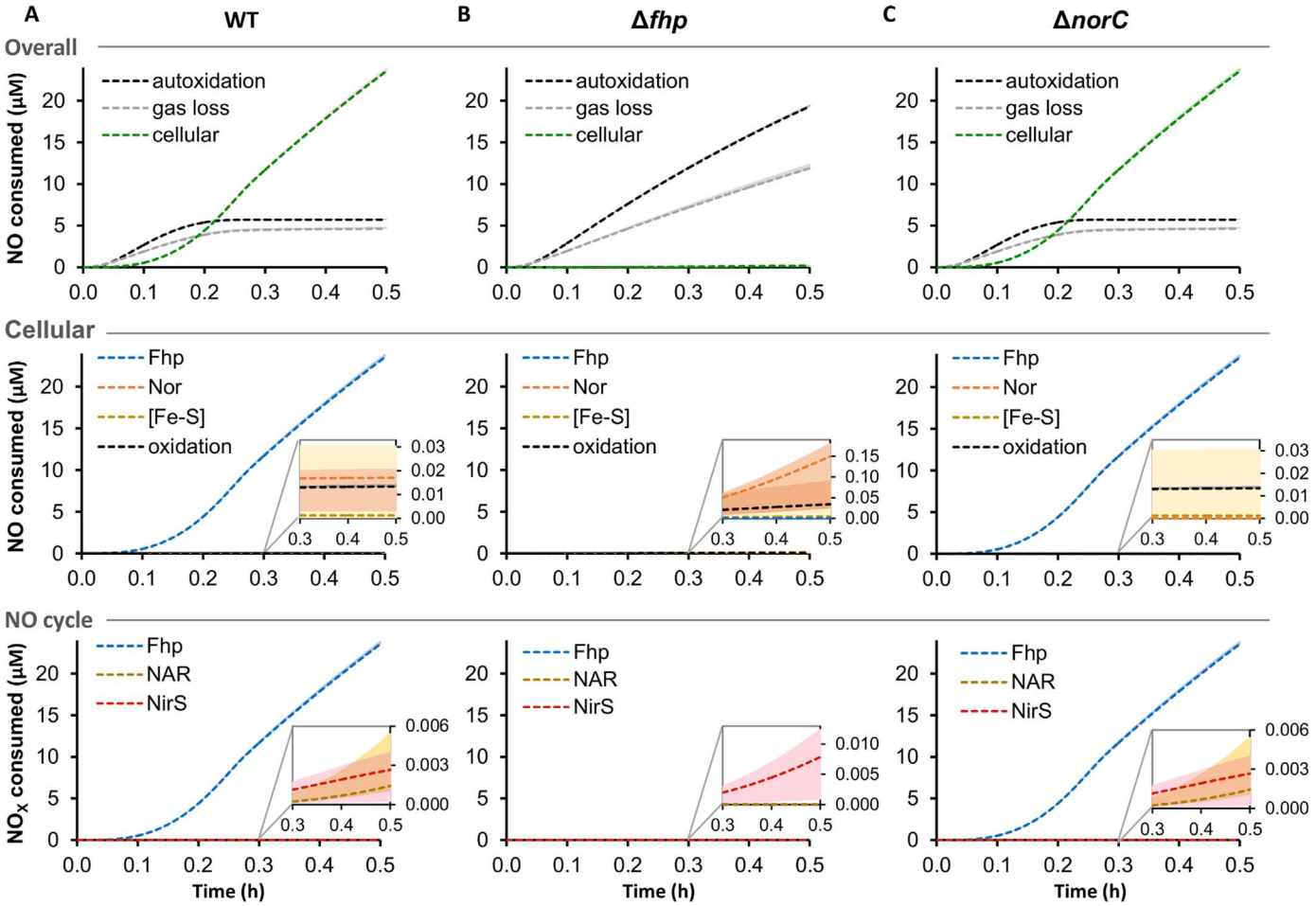

Fig. 3. Simulated flux through the NO biochemical network of *P. aeruginosa*. Using the ensemble of models, DPTA treatment (50 μM) of (A) WT, (B) Δ*fhp*, and (C) Δ*norC* PAO1 cultures was simulated, and the cumulative consumptions of NO by the major overall pathways (autoxidation in the media, loss to the gas phase, and cellular consumption) and the intracellular pathways (dioxygenation by Fhp, reduction by NorCB, [Fe-S] nitrosylation, and "oxidation", which includes the reaction of NO with O_2, superoxide, and hydroxyl radicals) were determined. In addition, the cumulative consumptions of NO, NO_2^-, and NO_3^- ("NO_X") through the three enzymes participating in the NO metabolic cycle (Fhp, NAR, and NirS) were calculated. Dashed lines are simulation results obtained using the best-fit model, with light shading of the same color representing the range of predictions among ensemble members. The insets are a zoomed-in region to show consumption values that are otherwise too small to view. (For interpretation of the references to color in this figure legend, the reader is referred to the web version of this article).

system forms a biochemical equivalent to "kicking the can down the road", where NO would be chemically pacified only to arise again at a future time. Such a scenario could be prevented if NO_2^- were processed by the assimilatory reductase, NirBD, which yields NH_3 rather than NO, or if NO were detoxified by NO reductase, NorCB, which yields N_2O rather than NO_3^- (Fig. 1). Given the data presented in Fig. 2, which demonstrated that Fhp was a major cellular consumption pathway under the conditions investigated here, we sought to assess whether aerobic *P. aeruginosa* cultures execute this NO cycle. To do this, we calculated the flux through each of the enzymes comprising the NO metabolic cycle, as well as the distribution of NO flux through all other available pathways, using the ensemble of viable models that we had constructed.

Treatment of WT PAO1 with 50 μM DPTA NONOate was simulated by the ensemble and the results were consistent with the large impact of Δ*fhp* on NO detoxification dynamics (Fig. 3A); Fhp was predicted to account for the majority of NO consumption, reaching ~24 μM NO by 0.5 h, compared to the ~5 μM NO consumed by autoxidation in the media and loss to the gas phase. Flux of NO through other pathways, such as [Fe-S] nitrosylation, was negligible, cumulatively accounting for less than 0.03 μM of NO consumed. Deletion of *fhp* from the ensemble eliminated the majority of cellular-related NO consumption, leaving autoxidation and escape to the gas phase as the two major pathways (Fig. 3B), though we note that flux through reactions that damage biomolecules were generally increased (*e.g.*, [Fe-S] nitrosylation increased to a maximum of 0.09 μM cumulative NO consumed). Removal of *norC* exhibited nearly the same metabolic flux distribution as WT (Fig. 3C).

In terms of the NO cycle, the calculated NO_X consumption by NAR and NirS in WT were orders of magnitude lower than that of Fhp, reaching a cumulative consumption (by 0.5 h post-dose) of only 0.001–0.005 μM NO_3^- and 0.0002–0.004 μM NO_2^-, respectively. Similar results were observed when simulating Δ*fhp* and Δ*norC* mutants, except for the complete elimination of NAR activity in Δ*fhp* due to the absence of NO_3^- supply by Fhp. These predictions suggested that the full cycle ($NO \rightarrow NO_3^- \rightarrow NO_2^- \rightarrow NO$) was not active under the conditions used here, and that it primarily stalled at NO_3^-. The low activities of the NO_3^- and NO_2^- reductases were likely a result of the aerobic environment, as these enzymes function optimally under anaerobic to microaerobic conditions (Schreiber et al., 2007; Arai, 2011). We therefore reasoned that progression through the NO cycle might occur as O_2 depleted as a result of respiration and cell growth.

2.3. Quantification of NO, NO_3^-, and NO_2^- dynamics in WT P. aeruginosa cultures

With the hypothesis that cell-mediated depletion of O_2 from the culture could activate the other branches of the NO cycle, we extended

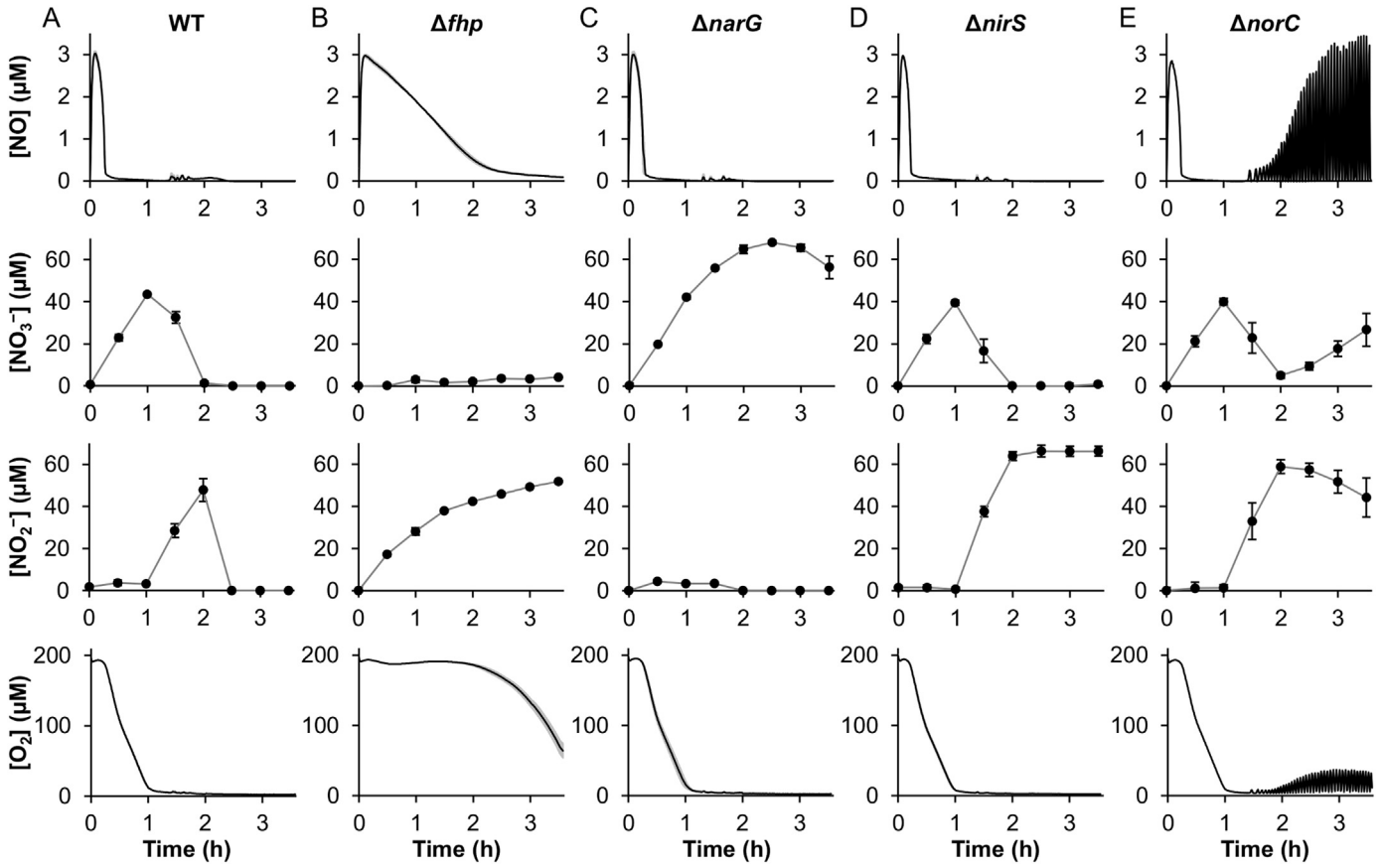

Fig. 4. Genetic analysis of NO metabolic cycle following DPTA treatment. (A) WT, (B) Δ*fhp*, (C) Δ*narG*, (D) Δ*nirS*, and (E) Δ*norC* PAO1 cultures at an initial OD_{600} of 0.05 were treated with 50 μM DPTA at time zero, and monitored for 3.5 h post-dose. Concentrations of NO and O_2 were measured continuously, whereas NO_2^- and NO_3^- were quantified every 0.5 h. Solid black lines (or circles) are the mean of 3 independent experiments, with gray shading (or error bars) representing the SEM. The exception is [NO] and [O_2] of Δ*norC*, which are data from one representative experiment because averaging multiple experiments obscures the oscillatory dynamics (see Fig. S11 for remaining Δ*norC* data).

the duration of experiments. Following relief of NO-induced respiratory inhibition, which occurred at ~0.25 h post DPTA treatment, O_2 was consumed rapidly and periodic quantification of [NO_2^-] and [NO_3^-] revealed that virtually all NO_2^- and NO_3^- generated from DPTA was consumed by 3.5 h post-treatment (Fig. 4A).

We note that the computational model constructed in the previous sections was not designed to account for the complexities associated with transitioning from an antimicrobial-induced bacteriostasis to an unstressed growing state. Therefore, computational analyses were not used to examine experimental data beyond 0.5 h, which was the final measured time point at which the cell density of the culture was not statistically higher than that of the initial time point (Fig. S4). We note that this functional constraint was also present in the predecessors of this model, which were constructed to examine NO stress networks in *E. coli* (Robinson and Brynildsen, 2013, 2016a, 2015). Furthermore, the *P. aeruginosa* model was not trained on experimental measurements from low-[O_2] conditions, which manifest as culture densities increase. Such O_2-limited conditions are of interest due to the diversity of O_2 levels encountered by *P. aeruginosa* during infections, and augmenting the model to account for those environmental conditions represents an area of future growth for this research.

For ~1 h after DPTA treatment, [NO_2^-] remained negligible, whereas [NO_3^-] increased rapidly to 43.5 ± 0.6 μM (Fig. 4A). This behavior was consistent with NO consumption being dominated by NO dioxygenase (Fhp), the main product of which is NO_3^-. The negligible production of NO_2^- during this period was attributed to the rapid consumption of NO by Fhp, which prevented appreciable NO_2^- generation from autoxidation, and the absence of NAR activity, which reduces NO_3^- to NO_2^-. Inspection of the corresponding WT [O_2] dynamics revealed a brief ~0.25 h period of NO-induced respiratory arrest, followed by resumption of O_2 consumption upon clearance of NO from the culture media. Despite having the culture open to the ambient air, the respiratory activity was sufficient to deplete O_2 by 1 h post-DPTA treatment, stabilizing at ~3 μM O_2. The depletion of O_2 from the culture coincided with a decrease in [NO_3^-], and an increase in [NO_2^-], indicating the initiation of NAR activity. Within an hour after NAR activity was observable, the concentration of NO_2^- rapidly decreased, which suggested that NirBD and/or NirS was active. However, this rapid consumption of NO_2^- was not matched by concurrent increases in NO or NO_3^-, which suggested that either NO_2^- was being converted by NirBD to NH_3 and/or the NO generated by NirS was being detoxified by NorCB, which generates N_2O.

2.4. Genetic investigation of NO, NO_3^-, and NO_2^- dynamics

We sought to determine the enzymes responsible for NO, NO_3^-, and NO_2^- reduction in NO-stressed *P. aeruginosa* cultures, which concomitantly would identify whether NirBD or NorCB were preventing the NO cycle. Given that the only appreciable source of NO_3^- could be Fhp, we hypothesized that negligible NO_3^- production would be observed in a Δ*fhp* culture treated with DPTA. As expected, when Δ*fhp* cultures were treated with DPTA, only trace levels of NO_3^- were observed, which confirmed that Fhp was the primary source of NO_3^- under these conditions (Fig. 4B). Notably, NO_2^- was generated at a rate similar to that observed in the absence of cells (Fig. S5), which suggested an active autoxidation pathway. Unlike WT, Δ*fhp* did not exhibit rapid NO_2^- reductase activity, where only a modest decrease in [NO_2^-] relative to the cell-free control was observed at later times (final [NO_2^-]=51.7 ± 0.6 μM for Δ*fhp* compared to the 58.9 ± 1.3 μM measured in the absence of cells). This could have resulted from NO-

mediated inhibition of NIR (Silvestrini et al., 1994), given that NO was cleared much slower from the Δ*fhp* culture than WT (> 2 h *vs*. ~0.25 h, respectively), or the higher [O_2] in the Δ*fhp* culture, which could inhibit NIR expression and/or activity (Arai, 2011). Further, since NIR expression is partially activated by NO_3^- (Schreiber et al., 2007; Arai, 2011), the lack of NO_3^- may have contributed to decreased NIR activity. Collectively, the results from NO-stressed Δ*fhp* demonstrated that Fhp was the source of NO_3^-.

In WT cultures, consumption of NO_3^- coincided with depletion of O_2 (Fig. 4A). Given that NAR activity in *P. aeruginosa* is known to function primarily under low-O_2 conditions (Hernandez and Rowe, 1987; Schreiber et al., 2007; Arai, 2011), we reasoned that one or more of the *P. aeruginosa* NARs were responsible for the observed NO_3^- consumption. To determine the enzyme(s) contributing to the measured NO_3^- consumption activity, DPTA treatment assays were conducted with Δ*narG*, which inactivates a membrane-bound cytoplasmic NO_3^- reductase, and Δ*napA*, which inactivates a periplasmic NO_3^- reductase (Schreiber et al., 2007; Arai, 2011; Zumft, 1997; Palmer et al., 2007; Van Alst et al., 2009b). Deletion of *napA* had a negligible effect on all measured metabolites (Fig. S6), whereas loss of NarG eliminated virtually all NO_3^- consumption (Fig. 4C). Consistent with the loss of NO_3^- consumption in Δ*narG* cultures, the corresponding production of NO_2^- was eliminated. This confirmed that the sharp increase in [NO_2^-] observed in DPTA-treated WT cultures at ~1 h post dose was caused by NAR, and attributed the effect specifically to NarGHI ([NO_2^-] dynamics of Δ*napA* were indistinguishable from those of WT).

With Fhp and NarGHI confirmed to be the respective NO_3^- and NO_2^- sources in NO-stressed *P. aeruginosa*, we sought to identify whether NirBD or NirS was responsible for NO_2^- consumption. If NirS were found to contribute to NO_2^- consumption, it would mean that NO was only temporarily deactivated to arise again later, whereas if NirBD were the major consumption pathway, NO detoxification by Fhp would be the first step in a non-cyclic NO deactivation pathway. The rapid decrease in [NO_2^-] during the WT DPTA treatment assay confirmed the presence of NIR activity, but held no information regarding the relative contributions of NirBD and NirS. To assess what portion of the observed NIR activity could be attributed to NirBD and NirS, DPTA treatment assays were conducted with Δ*nirS* and Δ*nirB* mutants. Deletion of *nirB* had a negligible effect on the measured [NO], [O_2], [NO_2^-], and [NO_3^-] compared to WT (Fig. S6), suggesting that NirBD was either not expressed or was inactive under the conditions studied. Conversely, NO_2^- consumption in the Δ*nirS* culture was almost entirely eliminated, where [NO_2^-] peaked similarly to WT at ~2 h post-DPTA dose, but remained steady at ~66 μM for the remainder of the assay (Fig. 4D). These data suggest that *P. aeruginosa* detoxifies NO with Fhp, only to have it appear again at a later time (when NirS reduces NO_2^- to NO). Further, the Δ*nirS* data in conjunction with that of WT, which showed that negligible amounts of NO, NO_3^-, or NO_2^- were present after 2.5 h (Fig. 4A), suggested that NO was being siphoned from the cycle and prevented from entering a second round of deactivation by Fhp. Possible pathways that could remove NO from the cycle were exchange with the gas phase, which was not rapid enough to explain the quantitative losses of NO, NO_3^-, and NO_2^-(given a k_La_{NO} of 8.6 h^{-1} and [NO] < 1 μM in the culture, the amount of NO_2^- that could be lost as NO to the gas phase over a span of 30 min would be under 1 μM×8.6 h^{-1}×0.5 h=4.3 μM NO, which is an order of magnitude less than the observed ~50 μM NO_2^- decrease), or NorCB, which reduces NO to N_2O.

In general, NORs require anaerobic or low-O_2 environments to function, as O_2 impairs their activity (Arai et al., 1995; Zumft, 1997; Gardner and Gardner, 2002). This is consistent with the initial DPTA-treatment assays conducted to validate the model predictions, where Δ*norC* NO consumption was indistinguishable from that of WT during the first 0.5 h post-DPTA dose (Fig. 2). However, after 1 h the [O_2] was ~3 μM, which are conditions more conducive to NOR activity. To assess whether NorCB prevented NO cycling, DPTA treatment assays were performed with Δ*norC*. During the first hour following DPTA treatment, Δ*norC* behaved identically to WT (Fig. 4E), which was expected given that the dissolved [O_2] had just reached a low level and NO_2^- had yet to be appreciably consumed. However, approximately 15 min later, the [NO] dynamics of Δ*norC* cultures began to deviate from that of WT, exhibiting sustained oscillations of increasing amplitude (Fig. 4E). The [NO] oscillations continued for the remaining duration of the assay (3.5 h post-DPTA treatment), at which point the amplitude had reached the initial peak height of ~3 μM NO. Similar oscillations were observed in [O_2], shifted slightly out of phase with those of [NO] (Fig. S7A), which was consistent with a previously-identified oscillatory mechanism driven by a competition between NO dioxygenase and respiratory cytochromes over the limited dissolved O_2 in the system (Robinson and Brynildsen, 2016a). Further, [NO_2^-] in the Δ*norC* culture did not drop as rapidly as WT, and the [NO_3^-] began increasing in Δ*norC* at the time when [NO_2^-] declined, whereas [NO_3^-] remained at undetectable levels in WT cultures after its initial clearance. These data confirmed that NorCB was the major pathway siphoning NO from the NO cycle prior to its second deactivation by Fhp.

2.5. Analysis of NO cycle initiated by NO_3^-

Results presented in Fig. 4 suggest that *P. aeruginosa* initially detoxifies NO to NO_3^- only to have it arise again later from NO_2^-. Within the assays presented thus far, NO is delivered to cultures by release from DPTA. In consideration of the kinetic release rate of DPTA, only ~30 μM of NO would have been left to be released from DPTA by 1.5 h post-dose, which corresponded to the time that NO briefly returned to WT cultures and Δ*norC* began exhibiting NO oscillations. Given this calculation, data from Δ*nirS*, and the magnitude of NO oscillations in Δ*norC*, it is reasonable to assume that NO_2^- consumption sustained the NO cycle and oscillations in Δ*norC*. However, to provide further experimental evidence that the NO cycle is driven by endogenous NO production, cultures of WT and Δ*norC P. aeruginosa* were treated with a single bolus of 100 μM NO_3^-(final concentration) at time zero (DPTA was not present), and the resulting [NO], [O_2], [NO_3^-], and [NO_2^-] were monitored for 3.5 h (Fig. 5).

For both strains, within the first 0.5 h of NO_3^- addition, there was no change in any of the measured metabolite concentrations except O_2, which was steadily depleted from the cultures. By 1 h post-dose, the [O_2] had stabilized at ~3 μM (~1.5% of the air-saturated O_2 concentration), and NAR activity began converting the NO_3^- to NO_2^-. Flux through the NO_3^- to NO_2^- arm of the cycle increased considerably between 1 and 1.5 h, as illustrated by large drops in [NO_3^-] and concurrent increases in [NO_2^-] for both strains. The rate of NO_2^- consumption greatly increased over the next 0.5 h for WT, where [NO_2^-] decreased to ~7 μM at 2 h post-NO_3^- treatment. Consistent with results from DPTA treatments, consumption of NO_2^- did not coincide with a comparable increase in NO for WT, and neither NO, NO_3^-, nor NO_2^- were detected at later time points. However, unlike WT, with Δ*norC* NO became detectable when NO_2^- began to accumulate, and its concentration oscillated (Fig. 5B). Oscillations in [O_2] that were slightly off-phase with [NO] were observed (Fig. S7B), NO_2^- consumption was slower than that of WT, and NO_3^- began to accumulate in Δ*norC* cultures. These data provide additional evidence that NO cycles in *P. aeruginosa* cultures when NorCB activity is absent, and that it is endogenously generated NO that contributes to this process.

2.6. Analysis of the period and amplitude of NO oscillations

The metabolic oscillations reported here for Δ*norC* cultures of *P. aeruginosa* resemble those of a previous study we performed on microaerobic NO detoxification (Robinson and Brynildsen, 2016a). However, there are notable differences in the oscillation dynamics,

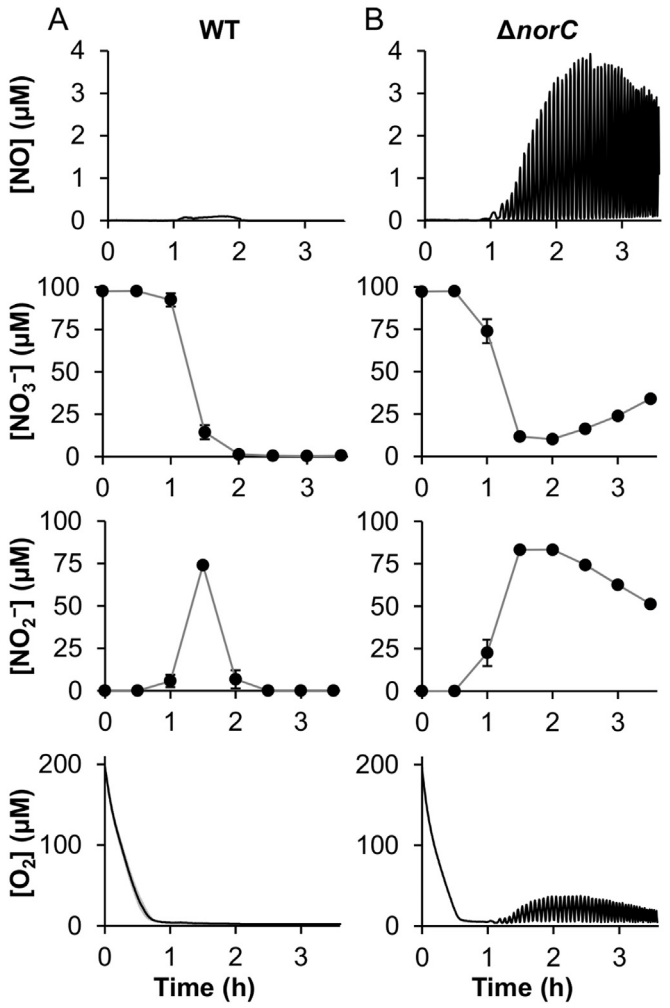

Fig. 5. Metabolic cycling of NO following treatment with NO_3^-. (A) WT and (B) Δ*norC* PAO1 cultures at an initial OD_{600} of 0.05 were treated with 100 μM $NaNO_3$ at time zero, and monitored for 3.5 h post-dose. Concentrations of NO and O_2 were measured continuously, whereas NO_2^- and NO_3^- were quantified every 0.5 h. Solid black lines (or circles) are the mean of 3 independent experiments, with gray shading (or error bars) representing the SEM. The exception is [NO] and [O_2] of Δ*norC*, which are data from one representative experiment because averaging multiple experiments obscures the oscillatory dynamics (see Fig. S10 for remaining Δ*norC* data).

especially with regard to amplitude and period. For example, from our previous study, the period and amplitude of the largest NO oscillation were approximately 10 min and 0.5 μM in *E. coli* populations cultured in environments where 10 μM [O_2] was the concentration in equilibrium with the surrounding atmosphere, whereas the period and amplitude of the largest oscillation in Δ*norC P. aeruginosa* populations cultured here (equilibrium [O_2] of 210 μM) was approximately 3 min and 3.4 μM, respectively. Further, in our previous study, we observed NO oscillations in WT *P. aeruginosa* populations cultured in environments where 50 μM [O_2] was the concentration in equilibrium with the surrounding atmosphere, and the period and amplitude of the largest oscillation was approximately 4 min and 0.35 μM. Since these differences in oscillation dynamics could be attributed to environmental or bacteria-associated factors, we sought to identify those variables with considerable influence on the oscillation properties. To do this, we turned to a minimal NO model that displays these metabolic oscillations from our previous study, and analyzed how varying the magnitude of parameters associated with environmental and bacteria-specific differences alter the period and amplitude of oscillations. Both *E. coli* and *P. aeruginosa* possess the necessary genetic components for oscillatory behavior (NOD and O_2-consuming respiratory cytochromes (Robinson and Brynildsen, 2016a)), but they differ in the number of these components (*E. coli* harbors three cytochromes, whereas *P. aeruginosa* has five (Keseler et al., 2013; Arai, 2011; Kanehisa et al., 2016)), as well as in the amino acid sequence and catalytic activity of their respective NODs (Frey and Kallio, 2003). The minimal model used for the oscillatory analysis is presented in Model S2.

To begin, we investigated how environmental variables affected oscillation dynamics, and focused specifically on the rate of NONOate disassociation and dissolved [O_2] that was in equilibrium with the surrounding atmosphere. The NONOate disassociation rate dictated the delivery of NO to cultures, and it is a function of pH, which was different between media used for *E. coli* and *P. aeruginosa* (pH=7.4 for *E. coli*/MOPS media, pH=7.0 for *P. aeruginosa*/BSM media). Interestingly, when this parameter was varied over a 4-fold range from its original value, a non-monotonic response was observed, with period and amplitude initially increasing as NO was delivered faster, only to decrease at a higher release rate (Fig. 6A). The [O_2] in equilibrium with the surrounding atmosphere affects O_2 transport into the culture and the maximum [O_2] that can be attained, and previous observations have shown that this variable has the capacity to eliminate or enable oscillations (Robinson and Brynildsen, 2016a). When the equilibrium [O_2] was varied within a 4-fold range, higher values produced oscillations with a shorter period and amplitude than those at lower values (Fig. 6B). Taken together, these simulation results suggest that the NONOate disassociation rate and equilibrium [O_2] exert considerable influence on the NO oscillation period and amplitude.

To explore variables that can vary between species or strains, we investigated parameters governing the activity of the respiratory cytochromes and NOD (Fig. 6B). For the cytochromes, we observed that increasing the affinity for O_2 (*e.g.*, decreasing associated K_m) increased the oscillation period and amplitude, whereas increasing the affinity for NO had the opposite effect. This can be rationalized by considering that O_2 and NO compete with one another for binding to the cytochromes, and the cytochromes outcompete NOD for O_2. With respect to NOD, increasing its affinity for NO increased the amplitude and period, whereas increasing its affinity for O_2 had the opposite effect. For O_2, increasing its affinity enables NOD to compete more effectively with the cytochromes for this common substrate, which one would expect to decrease the oscillation amplitude and period. The NOD affinity for NO in this context refers to the binding of NO with the O_2-bound form of NOD, leading to NO_3^- product formation, rather than the binding of NO to NOD prior to O_2, which is a process known in *E. coli* to inhibit NOD activity (Gardner et al., 2000). The increase in oscillation period and amplitude observed upon increasing NO affinity of NOD can be explained by the faster rate at which O_2-bound NOD is consumed, leaving more unbound NOD exposed for potential inhibition by NO. This parameter is therefore indirectly increasing the rate of NO-mediated NOD inhibition, resulting in larger [NO] peaks from which the bacteria are slower to recover.

Given that NO-mediated inhibition of NOD appeared to have an effect on oscillation dynamics, and because this inhibitory reaction has not yet been reported for the NOD of *P. aeruginosa*, Fhp, we explored a parameter directly governing this process ($k_{on,NO}$, the rate of inhibitory binding of NO to NOD). The NO binding rate was increased by two-fold and decreased to zero, to represent the possible absence of this process in *P. aeruginosa* (Fig. 6C). Interestingly, the oscillations were eliminated when the rate of NO binding was set to zero, suggesting that this inhibitory effect may play an important role in the oscillation mechanism. Since *P. aeruginosa* cultures were shown experimentally to exhibit oscillations, we hypothesize that, similar to *E. coli* Hmp, *P. aeruginosa* Fhp also experiences NO-mediated substrate inhibition; however, this effect requires experimental verification with biochemical assays.

Another important distinction between the previously observed oscillations and those reported here was the required deletion of NOR under the conditions investigated in this study. We therefore examined the effect of varying flux through a NOR reaction on the oscillation

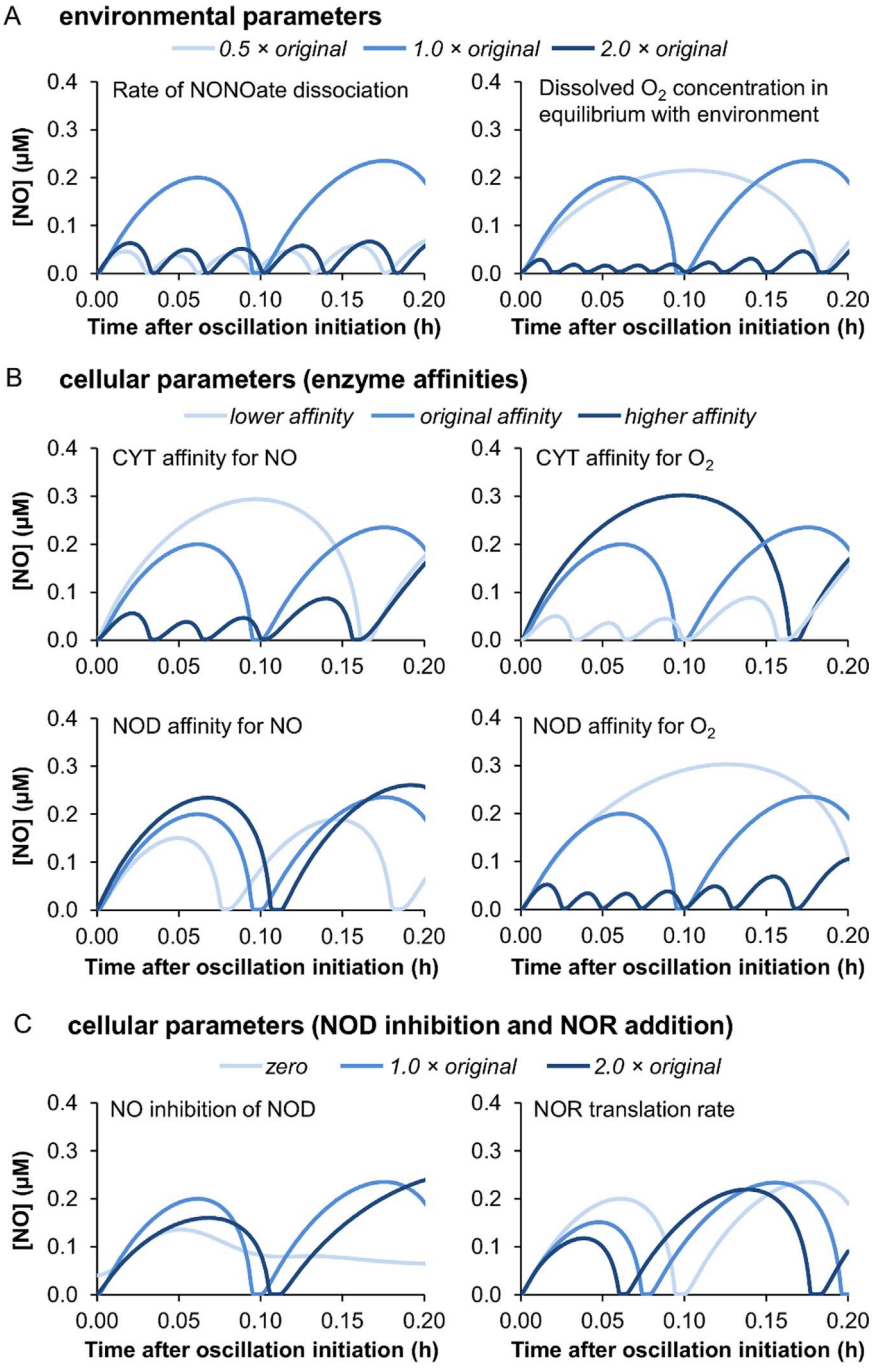

Fig. 6. Impact of environmental and cellular parameters on NO oscillation dynamics. The core oscillatory model from Robinson and Brynildsen (2016a) was used to simulate NO treatment and assess the effect of varying key model parameters on the resulting oscillations. To facilitate comparison of oscillations, the time-scale (*x*-axis) was shifted to reflect the time after oscillations began, rather than time after NONOate treatment. (A) Parameters related to culturing conditions were increased and decreased by two-fold of their original value: NONOate release rate ($k_{NONOate}$) and dissolved [O_2] in equilibrium with the environment ([O_2]$_{env}$). (B) Cellular parameters governing the binding affinity of NOD and CYT (high-affinity cytochrome) for NO and O_2 were varied within two-fold of their original value: on-rate of NO to CYT ($k_{on,NO}$), O_2 Michaelis constant for CYT ($K_{m,O2}$), on-rate of NO to O_2-bound NOD (k_{ox}), and on-rate of O_2 to NOD (k_{O2}). (C) Cellular parameters governing NO-mediated NOD inhibition ($k_{on,NO}$) and the expression of NOR ($k_{translate,NOR}$) were set to zero, their original value, or increased two-fold from their original value. Since NOR was not originally present in the core oscillatory model, the "original" value is derived from the full *E. coli* model. The core model, which includes the "original" values of all parameters described here, are presented in Model S2.

dynamics. Since NOR was absent from the minimal oscillation model, it was introduced by transferring all NOR-related reactions, parameters, and species from the full *E. coli* model (Robinson and Brynildsen, 2016a) to the minimal oscillating model. Flux through NOR was varied by changing the rate of NOR expression ($k_{translate,NOR}$) from zero to the original parameter value, and two-fold the original value (Fig. 6C). Increasing rates of NOR expression resulted in decreased oscillation amplitude and period, which is expected given that this enzyme serves as an additional NO sink. To provide additional experimental confirmation that NOR repress NO oscillations, we performed experiments with *E. coli* lacking NOR (Δ*norV*) under the same conditions as used in our previous study (50 μM DPTA NONOate, 10 μM O_2 environment) (Robinson and Brynildsen, 2016a). As predicted, the resulting oscillations within Δ*norV E. coli* cultures exhibited an increased period and amplitude relative to WT (approximately 14 min and 0.7 μM, respectively, for the maximum oscillation, a 40%

increase over the 10 min and 0.5 μM of WT) (Fig. S8). The considerable impact many of the parameters analyzed here had on the period and amplitude of oscillations suggests that these features should be expected to vary as a function of bacterial species and culturing conditions.

3. Discussion

P. aeruginosa are prevalent, opportunistic pathogens that are increasingly refractory to many antibiotics (Breidenstein et al., 2011; Gellatly and Hancock, 2013; Lyczak et al., 2000). Cystic fibrosis patients commonly develop *P. aeruginosa* infections within their airways, nosocomial infections (*e.g.*, ventilator-associated pneumonia) are often caused by *P. aeruginosa,* and *P. aeruginosa* is a frequent inhabitant of chronic, non-healing wounds (Driscoll et al., 2007; Winstanley et al., 2016; Govan and Deretic, 1996). The propensity for *P. aeruginosa* to form biofilms combined with both its innate and acquired resistance toward antibiotics prompted the Center for Disease Control to label multi-drug resistant *P. aeruginosa* as a "serious threat" to public health (Centers for Disease Control and Prevention, 2013). To address this threat, novel treatment modalities are needed (Gellatly and Hancock, 2013; Rasko and Sperandio, 2010), and one of those being explored focuses on NO (Barraud et al., 2006; Deppisch et al., 2016; Friedman et al., 2011; Miller et al., 2013; Yoon et al., 2006).

Due to the ability of NO to disperse *P. aeruginosa* biofilms and the importance of NO detoxification machinery to *P. aeruginosa* virulence (Kakishima et al., 2007; Arai and Iiyama, 2013), several groups have investigated the use of NO as an alternative to conventional antibiotics (Deppisch et al., 2016; Friedman et al., 2011; Miller et al., 2013; Yoon et al., 2006). Miller and colleagues observed a significant reduction in *P. aeruginosa* bacterial load in a rat model of cystic fibrosis with the use of inhaled, gaseous NO when compared to untreated controls (Miller et al., 2013). In a phase I clinical trial, gaseous NO reduced bacterial loads, which included *P. aeruginosa*, within the sputum of cystic fibrosis patients (Deppisch et al., 2016). In addition, Friedman and colleagues observed impressive growth inhibition of numerous Gram-positive and Gram-negative clinical isolates, which included *P. aeruginosa*, when NO-delivering nanoparticles were used in comparison to control particles (Friedman et al., 2011).

Bacterial NO stress networks are dominated by enzymes that rapidly consume NO, and thereby restrict its reactions with other pathways, such as those that lead to protein and DNA damage or metabolic dysfunction. In essence, this is analogous to substrates (*e.g.*, NO) failing to be converted into a desirable product (*e.g.*, inactive, nitrosylated Fe-S clusters) due to competing reactions (*e.g.*, detoxification by NO dioxygenase). To modulate such native pathways for the improvement of cellular properties, as is a typical endeavor in metabolic engineering, understanding how systems quantitatively function is enabling. In the case of NO and *P. aeruginosa*, previous studies have clearly linked this metabolite and its biochemical network to the pathogen's virulence (Kakishima et al., 2007; Barraud et al., 2006, 2009), and in the context of health and disease, a desirable cellular property would be limited NO flux through detoxification pathways, and increased flux through pathways that damage the pathogen. To enable such interventions, quantitative knowledge of *P. aeruginosa* NO metabolism is desirable much in the same way that quantitative knowledge of substrate metabolism is desirable for rational improvements to the production of chemicals.

Given the critical role of NO in the pathogenicity and biofilm lifestyle of *P. aeruginosa*, as well as its potential to treat *P. aeruginosa* infections (Deppisch et al., 2016; Friedman et al., 2011; Miller et al., 2013; Yoon et al., 2006), we constructed a kinetic model of the *P. aeruginosa* NO biochemical network. The model is a computational tool that enables NO distributions in *P. aeruginosa* cultures to be quantitatively analyzed (Fig. 3), and previous models of this type have been constructed for *E. coli* K-12 and enterohemorrhagic *E. coli* O157:H7 (Robinson and Brynildsen, 2013, 2016b). The utility of these models has been demonstrated by uncovering a novel kinetic regime in which NO detoxification machinery performs poorly (Robinson and Brynildsen, 2013), predicting dosing regimens that maximize bacteriostasis at prescribed NO payloads (Robinson et al., 2014b), identifying the mechanism through which loss of ClpP impairs *E. coli* NO defenses (Robinson and Brynildsen, 2015), and delineating the subnetwork responsible for NO and O_2 oscillations within microaerobic environments (Robinson and Brynildsen, 2016a). We anticipate that similar advances will be enabled by the *P. aeruginosa* NO model described here, and importantly, translation of the modeling approach we employed, which thus far has only been demonstrated in *E. coli* strains (Robinson and Brynildsen, 2016b), to a non-model organism is an important milestone for broader application of the methodology.

Using the model developed in this study, we sought to determine whether NO was cycled in *P. aeruginosa* cultures. We were intrigued by the possibility that NO would be temporarily deactivated only to arise again at a later time, and there is evidence that NO, NO_3^-, and NO_2^-, which comprise the metabolites of this potential cycle, are present in the lungs of cystic fibrosis patients (Hassett et al., 2002; Kolpen et al., 2014). Further, this NO cycle appears to be broadly distributed, where 217 species within the KEGG database possess the enzymatic capacity to execute such a cycle (NO dioxygenase, NO_3^- reductase, and NO-generating NO_2^- reductase) (Table S7) (Kanehisa et al., 2016). Recently, data supporting the existence of NO cycles in *Corynebacterium glutamicum* (Platzen et al., 2014) and *Streptomyces coelicolor* (Sasaki et al., 2016) have been obtained. In addition, NO cycling has been known to occur in plants (Igamberdiev et al., 2010) and mammals (Reutov and Sorokina, 1998), of which the latter includes the function of NO synthases. Computational analysis of NO detoxification by aerobic *P. aeruginosa* cultures (Fig. 3), which were used to ensure Fhp activity, indicated a metabolic block in the cycle at NO_3^-. That block was relieved as *P. aeruginosa* consumed O_2 to drive metabolism into a microaerobic regime, within which NO_3^- was converted into NO_2^-, and NO_2^- was consumed without production of any appreciable NO or NO_3^- (Fig. 4A). Using a genetic approach, we identified NorCB as the enzyme drawing flux out of the NO cycle, and in its deletion strain, Δ*norC*, high frequency oscillations in [NO] and [O_2] were observed. These oscillations, which resemble those that we previously observed for NO-stressed *P. aeruginosa* in low O_2 environments (Robinson and Brynildsen, 2016a), are indicative of an unbalanced competition for O_2 between Fhp and the aerobic terminal oxidases.

NO is a metabolite with many functions, which range from neuronal signaling and vasodilation to use as an antimicrobial by immune cells (Bogdan, 2001; Nathan, 1992; Pacher et al., 2007). NO also has an important role in the nitrogen cycle as an intermediate in denitrification (Zumft, 1997). At the intersection of pathogenesis and denitrification lies *P. aeruginosa*, which is a dangerous human pathogen that can perform denitrification. *P. aeruginosa* can generate NO, is attacked by NO, and uses NO as a signal for virulence factor expression and biofilm dispersal (Barraud et al., 2009; Van Alst et al., 2007; Silvestrini et al., 1990). Collectively, the work presented here provides a computational tool for the quantitative analysis of NO metabolism in *P. aeruginosa*, and experimental evidence establishing that *P. aeruginosa* prevents NO cycling with the use of NO reductase. In this study, planktonic cultures of *P. aeruginosa* were used, and there is certainly precedent for knowledge gained from planktonic investigations to be important within the biofilm lifestyle (for example, see (Amato and Brynildsen, 2014; Amato et al., 2013)). However, biofilms are far more complex, for example with the presence of nutrient gradients and significant growth heterogeneity, as compared to their planktonic counterparts, and it will be exciting to see how *P. aeruginosa* NO metabolism within these lifestyles quantitatively compares as the approaches used here are adapted and applied to biofilms in future research. We postulate that as more quantitative knowledge of *P. aeruginosa* NO metabolism is

gained, such understanding in time, could be translated into the development of novel anti-infectives for treatment of infections caused by this prevalent pathogen.

4. Materials and methods

4.1. Bacterial strains and knockout construction

4.1.1. Bacterial strains

P. aeruginosa PAO1 (ATCC 15692) was used in this study, and is referred to as the WT strain. Single gene deletion mutants were constructed from the WT PAO1 parent strain to inactivate NO dioxygenase (Δ*fhp*), NO reductase (Δ*norC*), assimilatory NO_2^- reductase (Δ*nirB*), dissimilatory NO_2^- reductase (Δ*nirS*), periplasmic NO_3^- reductase (Δ*napA*), or membrane-bound NO_3^- reductase (Δ*narG*). The strain of *E. coli* used in this study was a Δ*norV* mutant (lacking NO reductase) of MG1655, constructed in a previous study (Robinson and Brynildsen, 2013).

4.1.2. Construction of knockout mutants

P. aeruginosa mutants were constructed using the lambda Red recombinase system (Lesic and Rahme, 2008) to replace the target gene with a gentamicin resistance cassette (harboring gentamicin 3′-acetyltransferase; *aacC1*), abbreviated here as gm^R. Briefly, the gm^R cassette was cloned from the pAS03 plasmid (Shen et al., 2012) using Phusion High-Fidelity DNA Polymerase (New England Biolabs; NEB), with primers possessing flanking ~40 nt sequences that were homologous to the PAO1 genomic sequence upstream and downstream of the target gene to be deleted (see Table S8A for knockout primers used in this study). Two additional PCRs were performed to amplify ~400–600 nt regions upstream and downstream of the target gene. An overlap extension PCR (Kuwayama et al., 2002) was used to combine the 3 DNA fragments (the upstream and downstream homology regions, and the fragment possessing the gm^R cassette), and amplify the joined product. The joined DNA product was gel-purified (Qiagen), eluted in DI H_2O, and stored at −20 °C.

WT PAO1 cells were made electrocompetent, and transformed (see Section 4.1.3 for further detail) with the pUCP18-RedS plasmid, which encodes for the lambda Red recombinase system (Lesic and Rahme, 2008). Transformants were plated on LB + agar plates containing 100 μg/mL carbenicillin to select for positive clones. The PAO1 pUCP18-RedS cells were again made electrocompetent, except growth was conducted in the presence of 100 μg/mL carbenicillin, and the cells were induced with 10 mM L-arabinose overnight to activate expression of the lambda Red system. Electrocompetent cells were transformed with ≥500 ng of the purified DNA product, and plated on LB+agar plates containing 30 μg/mL gentamicin. Colonies were selected from the plate, and re-streaked on LB+300 mM sucrose plates to remove the pUCP18-RedS plasmid, where counter-selection was enabled by the presence of the *sacB* gene on the plasmid (Lesic and Rahme, 2008). Positive clones were verified with colony PCR, using two sets of primers: one set with both forward and reverse primers homologous to regions within the targeted gene to confirm absence of the deleted gene in the mutant, and another with a forward primer upstream of the gene and reverse primer within the gm^R cassette to confirm proper genomic location of the inserted gm^R cassette (see Table S8B for the list of verification primers used in the present study).

4.1.3. Plasmid and DNA transformation

PAO1 cells (from −80 °C frozen stock) were grown for 16 h in 3 mL of LB at 37 °C and 250 rpm. For a gene deletion using the PAO1 pUCP18-RedS strain, the LB also contained 100 μg/mL carbenicillin, and 10 mM L-arabinose was added after 4 h of growth. The overnight culture was centrifuged (16,000×*g*) for 1 min, the supernatant discarded, and the pellet resuspended in 1 mL of room-temperature, 300 mM sucrose (dissolved in D.I. H_2O and filter-sterilized)—a solution commonly used to make *P. aeruginosa* electrocompetent (Siryaporn et al., 2014; Lesic and Rahme, 2008). The centrifugation and resuspension were repeated for 3 additional iterations, after which the pellet was resuspended in 100 μL of the sucrose solution. Purified plasmid or linear DNA was added to the cellular resuspension, and mixed gently with pipetting. The mixture was transferred to a 2 mm-gap electroporation cuvette, and electroporated at 2.5 kV. Immediately after electroporation, 1 mL of room-temperature LB was added to the cuvette, mixed gently by pipette, and transferred to a test tube. The cells were incubated at 37 °C and 250 rpm for 10 min, after which they were centrifuged and washed with fresh LB to eliminate residual sucrose, which inhibits growth of cells possessing the pUCP18-RedS plasmid harboring the *sacB* gene. Cells were again transferred to a test tube, and incubated at 37 °C and 250 rpm for 3 h, after which they were plated on LB+agar plates containing the appropriate selection marker.

4.2. Growth media and chemicals

Rich media used in this study was LB Broth (BD Difco). The minimal media used for *P. aeruginosa* was basal salts media (BSM) (30.8 mM K_2HPO_4, 19.3 mM KH_2PO_4, 15.0 mM $(NH_4)_2SO_4$, 1 mM $MgCl_2$, and 2 μM $FeSO_4$) (Wolff et al., 1991) supplemented with 15 mM succinate as the sole carbon source (referred to as "BSM" throughout the text). For experiments involving *E. coli*, the minimal media used was MOPS [3-(N-morpholino)propanesulfonic acid] media (Teknova) with 10 mM glucose as the sole carbon source. DPTA NONOate, (Z)-1-[N-(3-aminopropyl)-N-(3-ammoniopropyl)amino] diazen-1-ium-1,2-diolate (Cayman Chemical), was used as a chemical NO donor, which dissociates with a half-life of approximately 1 h at pH 7.0 and 37 °C to release 2 mol of NO per mol of parent compound. Antibiotics used were gentamicin (30 μg/mL) and carbenicillin (100 μg/mL). Unless noted otherwise, all chemical and media components were purchased from Sigma Aldrich or Fisher Scientific, and were autoclaved (LB media) or filter-sterilized (0.2 μm filters) prior to use.

4.3. DPTA and NO_3^- treatment assays

One mL of LB was inoculated with a scrape of frozen −80 °C PAO1 cells, and grown overnight (16 h) at 37 °C and 250 rpm. After overnight growth, the culture was mixed gently with a pipette to disrupt cell clumps, and 200 μL was removed to inoculate 20 mL of fresh BSM in a 250 mL baffled shake flask. The flask culture was incubated at 37 °C and 250 rpm until it reached an OD_{600} of 0.2, at which point 8 mL were removed and transferred to 1.5 mL microcentrifuge tubes. The cells were centrifuged at 17,000×*g* for 1 min, the supernatant was removed, and the pellets were resuspended and combined in 1 mL of fresh, pre-warmed (37 °C) BSM. The cell resuspension was used to inoculate 10 mL of fresh, pre-warmed BSM in a bioreactor to an OD_{600} of 0.05, after removing an equivalent volume (to maintain 10 mL total). Immediately after inoculation, bioreactor cultures were treated with 50 μM DPTA NONOate or 100 μM $NaNO_3$.

DPTA treatment of Δ*norV E. coli* was performed identically as described previously (Robinson and Brynildsen, 2016a). Briefly, 1 mL of LB media was inoculated with a scrape from a −80 °C frozen stock, and grown at 37 °C and 250 rpm for 4 h. 10 μL of LB culture was transferred to fresh MOPS media, and grown at 37 °C and 250 rpm in a hypoxic chamber (Coy Laboratory Products) overnight (16 h). The chamber environment was maintained at an O_2 level to achieve a dissolved [O_2] in media at equilibrium with the environment of 10 μM, and contained approximately 0.2% (2000 ppm) CO_2, and the balance N_2. A 250 mL baffled shake-flask with 20 mL of fresh MOPS media was inoculated to an OD_{600} of 0.01 with the overnight culture, and grown at 37 °C and 250 rpm in the chamber. Upon reaching and OD_{600} of 0.2, the flask culture was used to inoculate 10 mL fresh MOPS media in the

bioreactor (operated in the hypoxic chamber) to an OD_{600} of 0.05, and the bioreactor culture was treated immediately with 50 μM DPTA NONOate.

4.4. Bioreactor apparatus

The bioreactor apparatus used to facilitate continuous measurements of [NO] and [O_2] was adopted from a setup in a previous study (Robinson and Brynildsen, 2016a), and consisted of a 50 mL polypropylene conical tube containing 10 mL of media, open to the ambient air, and magnetically stirred with an ethanol-sterilized (soaked in 70%/30% ethanol/D.I. H_2O for >1 h) stir bar. The conical tube was suspended in a magnetically-stirred water bath, maintained at 37 °C with a stirring hotplate. The apparatus in its entirety was operated within a biological safety cabinet (Class II, Type A2 Biological Safety Cabinet, Labconco), except for the experiments conducted with *E. coli*, for which the bioreactor apparatus was operated in a hypoxic chamber (described in the section above).

4.5. Quantification of NO and O_2 concentrations

[NO] and [O_2] in bioreactor cultures were monitored continuously (≥1 reads/s) throughout assays, using a 2 mm ISO-NOP sensor (World Precision Instruments) and a fiber-optic FireStingO_2 robust miniprobe (PyroScience), respectively.

4.6. Quantification of NO_2^- and NO_3^- concentrations

[NO_2^-] and [NO_3^-] were measured using the Nitrate/Nitrite Colorimetric Assay Kit (Cayman Chemical), which is based on a Griess assay. Samples of 300 μL were removed from the culture, immediately sterile-filtered (0.22 μm Millex syringe-driven filter, Millipore) into sterile, 1.5 mL microcentrifuge tubes, and stored on wet ice until the end of the assay (when all samples had been collected), at which point samples were moved to a refrigerator (4 °C). The presence of unreacted DPTA in the culture filtrate prevented immediate quantification of [NO_2^-] and [NO_3^-], because Griess assays involve a pH reduction (Tsikas, 2007), which causes instantaneous release of NO from unreacted DPTA, which would rapidly autoxidize to form NO_2^-, NO_3^-, or escape to the gas phase. To accurately account for contributions of unreacted DPTA to NO_2^- and NO_3^- measurements, two steps were taken: (1) samples were stored for at least 24 h before processing, which provided sufficient time for the remaining DPTA to release NO, and for that NO to form NO_2^- and NO_3^-, and (2) a standard curve was generated by adding different concentrations of DPTA (0, 2, 5, 10, 15, 20, 30, and 50 μM) to separate aliquots of growth media (BSM at 37 °C) at the beginning of DPTA treatment assays. These standard curve samples were stored under identical conditions (4 °C) for a similar duration as the samples obtained from the DPTA treatment assay, and all samples were assayed for NO_2^- and NO_3^- concentrations simultaneously. The DPTA standards yielded a linear calibration curve, relating [DPTA] to [NO_2^-] and [NO_3^-] (Fig. S9). Based on the DPTA dissociation rate, which was determined from the [NO] curve measured in cell-free media (see Section 4.8.3), the amount of DPTA remaining in the culture at each time point was calculated, and the corresponding concentration of NO_2^- and NO_3^-, as determined from the standard curves, was subtracted from the measured values.

4.7. Model construction

Using an existing *E. coli* K-12 MG1655 model as a template (Robinson and Brynildsen, 2016a), the *P. aeruginosa* PAO1 kinetic model was constructed following a procedure that was recently employed to generate a quantitative model of NO stress in enterohemorrhagic *E. coli* O157:H7 (Robinson and Brynildsen, 2016b). Briefly, all reactions and parameters classified as organism-independent (*e.g.*, glutathione nitrosation, N_2O_3 hydrolysis) remained unchanged, whereas organism-specific components such as enzymes, metabolites, and transcriptional regulatory interactions were added, removed, or changed in accordance with the available body of literature on *P. aeruginosa* physiology (Arai et al., 2005, 2014; Schreiber et al., 2007; Arai, 2011; Zumft, 1997; Silvestrini et al., 1994, 1990; Carlson et al., 1982; Cutruzzola et al., 1997, 2001; Frey et al., 2002; Fukumori et al., 1985; SooHoo and Hollocher, 1991; Shapleigh et al., 1987; Kawakami et al., 2010). We note a difference in the pH of the growth media used for *P. aeruginosa* compared to that of *E. coli* (7.0 for *P. aeruginosa* grown in BSM media, 7.4 for *E. coli* grown in MOPS minimal media). Given that the magnitude of this pH difference was small, we assumed that it would only influence the system through its impact on the DPTA NONOate dissociation rate, which was a parameter that was optimized using data from cell-free experiments (Fig. S2).

A BLAST analysis was conducted for each of the enzymes in the original *E. coli* model to assess the amino acid sequence similarities with the corresponding *P. aeruginosa* homologues, if one existed (Table S9). Although *P. aeruginosa* possessed homologues for most (16 out of 20) of the enzymes, the amino acid sequences were not highly conserved, with a maximum similarity of ~80% for the iron-sulfur cluster assembly protein IscU. Given the relatively low sequence similarity among homologous proteins, their associated rate constants were released to be optimized during the initial model training process. The absolute concentrations of metabolites, biomolecules, and enzymes were unavailable for *P. aeruginosa*, and were therefore also released for optimization. Model parameters and species concentrations that were released for optimization were allowed to vary with bounds that were approximated based on literature data available for those components or functions in different bacterial species and/or different experimental conditions (Tables S4–S6).

In addition to releasing parameter values, the model adaptation process also required changes to the network structure (*i.e.*, addition/removal of reactions or changes to their stoichiometry). The *P. aeruginosa* O_2-respiration machinery differs greatly from that of *E. coli* (see Section 2.1.1 and refs (Keseler et al., 2013; Arai, 2011; Kanehisa et al., 2016)). Therefore, the *E. coli* cytochrome ubiquinol oxidases were removed and replaced with the five *P. aeruginosa* oxidases (Cyo, CIO, Cbb3-1, Cbb3-2, and Aa3), where ubiquinol served as the electron donor for Cyo and CIO, whereas Cbb3-1, Cbb3-2, and Aa3 received electrons from cytochrome *c*.

The other network region requiring substantial changes to architecture involved the denitrification reactions and transcriptional regulation of the involved enzymes. Whereas NO_2^- and NO_3^- reductases were omitted from the *E. coli* model, the *P. aeruginosa* NO_2^- reductases (NH_3-forming NirBD and NO-forming NirS) and NO_3^- reductases (NarGHI and NapAB, both NO_2^--forming) were incorporated into the present model. Transcriptional regulation of the main NO detoxification enzymes in *P. aeruginosa* (NOD: Fhp and NOR: NorCB) is similar to that of *E. coli*, in that NOD and NOR are strongly upregulated in the presence of NO. However, while Fhp appears to be regulated independently *via* the NO-responsive FhpR regulator (Arai et al., 2005), NorCB regulation is coupled with that of the NO_2^- and NO_3^- reductases (Schreiber et al., 2007; Arai, 2011). The expression of NorCB, NAR, and NIR are all regulated (directly or indirectly) by the anaerobic response regulator (ANR), which in turn controls expression of the denitrification response regulator (DNR) and a two-component nitrate sensing regulator (NarXL). These three transcription factors (ANR, DNR, and NarXL) are involved (to varying extents) in the regulation of NOR, NAR, and NIR (Fig. S1) (Schreiber et al., 2007; Arai, 2011). To take a mechanistic and physiologically-consistent approach, the ANR, DNR, and NarXL transcriptional regulators were included in the model (see Tables S2 and S3 for reactions and kinetic expressions involving the regulators).

4.8. Parameter optimization

4.8.1. Error minimization

Model parameters were optimized following a procedure described previously (Robinson and Brynildsen, 2016a; Adolfsen and Brynildsen, 2015). Briefly, model simulations were run by numerically integrating the governing system of ordinary differential equations using the Matlab *ode15s* stiff ODE solver. The Matlab *lsqcurvefit* function was used to minimize the sum of the squared residuals (SSR) between model simulation data (y_{sim}) and experimental measurements (y_{meas}), normalized by the experimental variance (σ^2):

$$SSR' = \sum_{i=1}^{n} \frac{(y_{i,meas} - y_{i,sim})^2}{\sigma_{i,meas}^2} \quad (1)$$

where SSR′ represents the variance-normalized SSR. To improve coverage of the solution space, the minimization was repeated for 1000 iterations, where each iteration began with a different set of randomized initial guess values for the varied parameters, from within their allowed bounds.

4.8.2. Estimation of parametric uncertainty

To estimate confidence in the optimized parameter values after the initial SSR′ minimization process, and in some cases identify improved optimal solutions, a subsequent Markov chain Monte Carlo (MCMC) procedure was employed (Robinson and Brynildsen, 2016a) using the *MCexp* function from the HYPERSPACE software package (Zamora-Sillero et al., 2011). The SSR′ was used as the cost function, and the algorithm was limited to 10,000 parameter evaluations (individual model simulations). Relative quality of fit for each of the parameter sets was quantified by the evidence ratio (ER), which is derived from the Akaike Information Criterion (AIC) (Hurvich and Tsai, 1989; Turkheimer et al., 2003):

$$AIC_{c,i} = n \ln\left(\frac{SSR_i'}{n}\right) + 2k + \frac{2k(k+1)}{n-k-1} \quad (2)$$

$$\Delta_i = AIC_{c,i} - \min(AIC_c) \quad (3)$$

$$w_i = \frac{\exp\left(-\frac{\Delta_i}{2}\right)}{\sum_{i=1}^{P} \exp\left(-\frac{\Delta_i}{2}\right)} \quad (4)$$

$$ER_i = \frac{w_{best}}{w_i} \quad (5)$$

where n is the number of data points, k is the number of fit parameters (plus one, due to the estimation of the SSR (Turkheimer et al., 2003)), w_i is the Akaike weight of parameter set i, w_{best} is the weight of the best-fit (minimum AIC) parameter set, and P is the total number of parameter sets being compared. Parameter sets with an ER ≥10 (less than 10% as likely as the best-fit set) were discarded from further analyses (Robinson and Brynildsen, 2016a; Adolfsen and Brynildsen, 2015).

4.8.3. Model training and ensemble generation

Model parameters were optimized in three different groups or modules: (1) extracellular, (2) respiration, and (3) remaining intracellular and NO detoxification/repair. The extracellular module was optimized first, and included three parameters: $k_{NONOate,DPTA}$, $k_{NO\text{-}O2}$, and $k_L a_{NO}$, which governed the dissociation rate of DPTA, the rate of NO autoxidation, and the rate of NO exchange with the gas phase, respectively. The volumetric mass transfer coefficient governing O_2 exchange with the gas phase, $k_L a_{O2}$, was determined independently by measuring dissolved [O_2] in cell-free growth media following N_2-purging, as described previously (Robinson and Brynildsen, 2013). The three extracellular parameters were trained on half-hourly measurements of [NO], [NO_2^-], and [NO_3^-] in cell-free BSM bioreactors treated with 50 μM DPTA, over the course of 2 h (Table S4). After the initial SSR′ minimization, the best-fit parameter sets (with ER < 10) were used as initial points in a subsequent MCMC analysis, yielding an ensemble of viable models (all ER < 10) differing only in the values of the three extracellular parameters. The confidence interval (CI) of each parameter was calculated as the range (min–max) of that parameter value among the ensemble members.

The respiratory module was optimized second, and included parameters governing concentrations and catalytic activities (*e.g.*, k_{cat}, K_m) of the NADH dehydrogenases, respiratory cytochromes, and their associated substrates and products, where a total of 27 parameters were optimized. The parameters were trained on dissolved [O_2] measurements of bioreactor cultures immediately after inoculation of WT PAO1 cells to an OD_{600} of 0.05 (in the absence of DPTA treatment) (Table S5). The concentration of O_2 was measured continuously, but only for 10 min post-inoculation, to avoid growth-related effects not captured by the model. Since the three extracellular parameters optimized previously ($k_{NONOate,DPTA}$, $k_{NO\text{-}O2}$, and $k_L a_{NO}$) have no effect on the system in the absence of NO, they were fixed to their best-fit values during the optimization of the respiratory parameters. A subsequent MCMC analysis was performed with the 27 respiration parameters to generate an ensemble of models, and quantify the corresponding parameter CIs.

After training of the extracellular and respiratory parameters, the remaining intracellular parameters—the majority of which included those related to NO stress, detoxification, and repair—were optimized. A total of 137 parameters were released to be optimized on experimental measurements of [NO], [O_2], [NO_2^-], and [NO_3^-] in WT PAO1 cultures treated with 50 μM DPTA for 30 min (Table S6). [NO] and [O_2] were measured continuously, whereas [NO_2^-] and [NO_3^-] were measured immediately after DPTA treatment, and at 30 min post-treatment. In addition to randomly initializing the 137 parameters at the start of each optimization iteration, the previously trained extracellular and respiratory parameters were set to values randomly selected from their respective ensembles. In this way, the uncertainties of the extracellular and respiratory parameter values were incorporated into the optimization process, rather than fixing them to single values. Furthermore, in the subsequent MCMC analysis of the 137 intracellular parameters, the extracellular and respiratory parameters were also permitted to vary (within their CIs), to enable a more complete exploration of the viable parameter space (Table S6).

Acknowledgements

We thank Professors Zemer Gitai and Albert Siryaporn for technical assistance with *P. aeruginosa,* and Anna Ren and Ismael Catovic for their initial work on the model. This work was supported by the National Science Foundation (CBET-1453325), and Princeton University (Forese Family Fund for Innovation, Lidow Senior Thesis Fund, start-up funds).

Appendix A. Supporting information

Supplementary data associated with this article can be found in the online version at doi:10.1016/j.ymben.2017.03.006.

References

Adolfsen, K.J., Brynildsen, M.P., 2015. A kinetic platform to determine the fate of hydrogen peroxide in Escherichia coli. PLoS Comput. Biol. 11 (11).
Allen, R.C., Popat, R., Diggle, S.P., Brown, S.P., 2014. Targeting virulence: can we make evolution-proof drugs? Nat. Rev. Microbiol. 12 (4), 300–308.
Amato, S.M., Brynildsen, M.P., 2014. Nutrient transitions are a source of persisters in Escherichia coli biofilms. PLoS One 9 (3), e93110.
Amato, S.M., Orman, M.A., Brynildsen, M.P., 2013. Metabolic control of persister formation in Escherichia coli. Mol. Cell 50 (4), 475–487.
Arai, H., 2011. Regulation and function of versatile aerobic and anaerobic respiratory metabolism in Pseudomonas aeruginosa. Front. Microbiol. 2, 103.

Arai, H., et al., 2014. Enzymatic characterization and in vivo function of five terminal oxidases in Pseudomonas aeruginosa. J. Bacteriol. 196 (24), 4206–4215.
Arai, H., Iiyama, K., 2013. Role of nitric oxide-detoxifying enzymes in the virulence of Pseudomonas aeruginosa against the silkworm, Bombyx mori. Biosci. Biotechnol. Biochem. 77 (1), 198–200.
Arai, H., Igarashi, Y., Kodama, T., 1995. The structural genes for nitric oxide reductase from Pseudomonas aeruginosa. Biochim. Biophys. Acta 1261 (2), 279–284.
Arai, H., Hayashi, M., Kuroi, A., Ishii, M., Igarashi, Y., 2005. Transcriptional regulation of the flavohemoglobin gene for aerobic nitric oxide detoxification by the second nitric oxide-responsive regulator of Pseudomonas aeruginosa. J. Bacteriol. 187 (12), 3960–3968.
Arat, S., Bullerjahn, G.S., Laubenbacher, R., 2015. A network biology approach to denitrification in Pseudomonas aeruginosa. PLoS One 10 (2), e0118235.
Bagci, E.Z., Vodovotz, Y., Billiar, T.R., Ermentrout, B., Bahar, I., 2008. Computational insights on the competing effects of nitric oxide in regulating apoptosis. PLoS One 3 (5).
Baquero, F., Martinez, J.L., Canton, R., 2008. Antibiotics and antibiotic resistance in water environments. Curr. Opin. Biotechnol. 19 (3), 260–265.
Barraud, N., et al., 2006. Involvement of nitric oxide in biofilm dispersal of Pseudomonas aeruginosa. J. Bacteriol. 188 (21), 7344–7353.
Barraud, N., et al., 2009. Nitric oxide signaling in Pseudomonas aeruginosa biofilms mediates phosphodiesterase activity, decreased cyclic di-GMP levels, and enhanced dispersal. J. Bacteriol. 191 (23), 7333–7342.
Bogdan, C., 2001. Nitric oxide and the immune response. Nat. Immunol. 2 (10), 907–916.
Bowman, L.A.H., McLean, S., Poole, R.K., Fukuto, J.M., 2011. The diversity of microbial responses to nitric oxide and agents of nitrosative stress: close cousins but not identical twins. Adv. Microb. Physiol. 59 (59), 135–219.
Breidenstein, E.B.M., de la Fuente-Nunez, C., Hancock, R.E.W., 2011. Pseudomonas aeruginosa: all roads lead to resistance. Trends Microbiol. 19 (8), 419–426.
Carlson, C.A., Ferguson, L.P., Ingraham, J.L., 1982. Properties of dissimilatory nitrate reductase purified from the denitrifier Pseudomonas aeruginosa. J. Bacteriol. 151 (1), 162–171.
Cegelski, L., Marshall, G.R., Eldridge, G.R., Hultgren, S.J., 2008. The biology and future prospects of antivirulence therapies. Nat. Rev. Microbiol. 6 (1), 17–27.
Centers for Disease Control and Prevention (CDC) UDoHaHS, 2013. Antibiotic Resistance Threats in the United States.
Chou, W.K., Brynildsen, M.P., 2016. A biochemical engineering view of the quest for immune-potentiating anti-infectives. Curr. Opin. Chem. Eng. 14, 82–92.
Chowdhury, A., Zomorrodi, A.R., Maranas, C.D., 2014. k-OptForce: integrating kinetics with flux balance analysis for strain design. PLoS Comp. Biol. 10 (2).
Cole, J., 1996. Nitrate reduction to ammonia by enteric bacteria: redundancy, or a strategy for survival during oxygen starvation? FEMS Microbiol. Lett. 136 (1), 1–11.
Cutruzzola, F., et al., 2001. The nitrite reductase from Pseudomonas aeruginosa: essential role of two active-site histidines in the catalytic and structural properties. Proc. Natl. Acad. Sci. USA 98 (5), 2232–2237.
Cutruzzola, F., Arese, M., Grasso, S., Bellelli, A., Brunori, M., 1997. Mutagenesis of nitrite reductase from Pseudomonas aeruginosa: tyrosine-10 in the c heme domain is not involved in catalysis. FEBS Lett. 412 (2), 365–369.
Darling, K.E., Evans, T.J., 2003. Effects of nitric oxide on Pseudomonas aeruginosa infection of epithelial cells from a human respiratory cell line derived from a patient with cystic fibrosis. Infect. Immun. 71 (5), 2341–2349.
Deppisch, C., et al., 2016. Gaseous nitric oxide to treat antibiotic resistant bacterial and fungal lung infections in patients with cystic fibrosis: a phase I clinical study. Infection.
Drenkard, E., Ausubel, F.M., 2002. Pseudomonas biofilm formation and antibiotic resistance are linked to phenotypic variation. Nature 416 (6882), 740–743.
Driscoll, J.A., Brody, S.L., Kollef, M.H., 2007. The epidemiology, pathogenesis and treatment of Pseudomonas aeruginosa infections. Drugs 67 (3), 351–368.
Escaich, S., 2008. Antivirulence as a new antibacterial approach for chemotherapy. Curr. Opin. Chem. Biol. 12 (4), 400–408.
Frey, A.D., Kallio, P.T., 2003. Bacterial hemoglobins and flavohemoglobins: versatile proteins and their impact on microbiology and biotechnology. FEMS Microbiol. Rev. 27 (4), 525–545.
Frey, A.D., Farres, J., Bollinger, C.J., Kallio, P.T., 2002. Bacterial hemoglobins and flavohemoglobins for alleviation of nitrosative stress in Escherichia coli. Appl. Environ. Microbiol. 68 (10), 4835–4840.
Friedman, A., et al., 2011. Susceptibility of Gram-positive and -negative bacteria to novel nitric oxide-releasing nanoparticle technology. Virulence 2 (3), 217–221.
Fukumori, Y., Nakayama, K., Yamanaka, T., 1985. Cytochrome c oxidase of Pseudomonas AM 1: purification, and molecular and enzymatic properties. J. Biochem. 98 (2), 493–499.
Gardner, A.M., Gardner, P.R., 2002. Flavohemoglobin detoxifies nitric oxide in aerobic, but not anaerobic, Escherichia coli – evidence for a novel inducible anaerobic nitric oxide-scavenging activity. J. Biol. Chem. 277 (10), 8166–8171.
Gardner, A.M., Martin, L.A., Gardner, P.R., Dou, Y., Olson, J.S., 2000. Steady-state and transient kinetics of Escherichia coli nitric-oxide dioxygenase (flavohemoglobin). The B10 tyrosine hydroxyl is essential for dioxygen binding and catalysis. J. Biol. Chem. 275 (17), 12581–12589.
Gardner, P.R., 2005. Nitric oxide dioxygenase function and mechanism of flavohemoglobin, hemoglobin, myoglobin and their associated reductases. J. Inorg. Biochem. 99 (1), 247–266.
Gardner, P.R., Gardner, A.M., Martin, L.A., Salzman, A.L., 1998. Nitric oxide dioxygenase: an enzymic function for flavohemoglobin. Proc. Natl. Acad. Sci. USA 95 (18), 10378–10383.
Gellatly, S.L., Hancock, R.E.W., 2013. Pseudomonas aeruginosa: new insights into pathogenesis and host defenses. Pathog. Dis. 67 (3), 159–173.
Govan, J.R., Deretic, V., 1996. Microbial pathogenesis in cystic fibrosis: mucoid Pseudomonas aeruginosa and Burkholderia cepacia. Microbiol. Rev. 60 (3), 539–574.
Hassett, D.J., et al., 2002. Anaerobic metabolism and quorum sensing by Pseudomonas aeruginosa biofilms in chronically infected cystic fibrosis airways: rethinking antibiotic treatment strategies and drug targets. Adv. Drug Del. Rev. 54 (11), 1425–1443.
Hauser, A.R., 2009. The type III secretion system of Pseudomonas aeruginosa: infection by injection. Nat. Rev. Microbiol. 7 (9), 654–665.
Hentzer, M., et al., 2003. Attenuation of Pseudomonas aeruginosa virulence by quorum sensing inhibitors. EMBO J. 22 (15), 3803–3815.
Hernandez, D., Rowe, J.J., 1987. Oxygen regulation of nitrate uptake in denitrifying Pseudomonas aeruginosa. Appl. Environ. Microbiol. 53 (4), 745–750.
Hu, T.M., Hayton, W.L., Mallery, S.R., 2006. Kinetic modeling of nitric-oxide-associated reaction network. Pharm. Res. 23 (8), 1702–1711.
Hurvich, C.M., Tsai, C.L., 1989. Regression and time-series model selection in small samples. Biometrika 76 (2), 297–307.
Hyduke, D.R., Jarboe, L.R., Tran, L.M., Chou, K.J.Y., Liao, J.C., 2007. Integrated network analysis identifies nitric oxide response networks and dihydroxyacid dehydratase as a crucial target in Escherichia coli. Proc. Natl. Acad. Sci. USA 104 (20), 8484–8489.
Igamberdiev, A.U., Bykova, N.V., Shah, J.K., Hill, R.D., 2010. Anoxic nitric oxide cycling in plants: participating reactions and possible mechanisms. Physiol. Plant. 138 (4), 393–404.
Kakishima, K., Shiratsuchi, A., Taoka, A., Nakanishi, Y., Fukumori, Y., 2007. Participation of nitric oxide reductase in survival of Pseudomonas aeruginosa in LPS-activated macrophages. Biochem. Biophys. Res. Commun. 355 (2), 587–591.
Kanehisa, M., Sato, Y., Kawashima, M., Furumichi, M., Tanabe, M., 2016. KEGG as a reference resource for gene and protein annotation. Nucleic Acids Res. 44 (D1), D457–D462.
Karr, J.R., et al., 2012. A whole-cell computational model predicts phenotype from genotype. Cell 150 (2), 389–401.
Kawakami, T., Kuroki, M., Ishii, M., Igarashi, Y., Arai, H., 2010. Differential expression of multiple terminal oxidases for aerobic respiration in Pseudomonas aeruginosa. Environ. Microbiol. 12 (6), 1399–1412.
Keseler, I.M., et al., 2013. EcoCyc: fusing model organism databases with systems biology. Nucleic Acids Res. 41 (D1), D605–D612.
Ketelboeter, L.M., Potharla, V.Y., Bardy, S.L., 2014. NTBC treatment of the pyomelanogenic Pseudomonas aeruginosa clinical isolate PA1111 inhibits pigment production and increases sensitivity to oxidative stress. Curr. Microbiol. 69 (3), 343–348.
Khodayari, A., Zomorrodi, A.R., Liao, J.C., Maranas, C.D., 2014. A kinetic model of Escherichia coli core metabolism satisfying multiple sets of mutant flux data. Metab. Eng. 25, 50–62.
Kolpen, M., et al., 2014. Nitric oxide production by polymorphonuclear leucocytes in infected cystic fibrosis sputum consumes oxygen. Clin. Exp. Immunol. 177 (1), 310–319.
Kuroki, M., Igarashi, Y., Ishii, M., Arai, H., 2014. Fine-tuned regulation of the dissimilatory nitrite reductase gene by oxygen and nitric oxide in Pseudomonas aeruginosa. Environ. Microbiol. Rep. 6 (6), 792–801.
Kuwayama, H., et al., 2002. PCR-mediated generation of a gene disruption construct without the use of DNA ligase and plasmid vectors. Nucleic Acids Res. 30 (2).
Lancaster, J.R., Jr., 2006. Nitroxidative, nitrosative, and nitrative stress: kinetic predictions of reactive nitrogen species chemistry under biological conditions. Chem. Res. Toxicol. 19 (9), 1160–1174.
Lesic, B., Rahme, L.G., 2008. Use of the lambda red recombinase system to rapidly generate mutants in Pseudomonas aeruginosa. BMC Mol. Biol. 9.
Lewis, R.S., Tamir, S., Tannenbaum, S.R., Deen, W.M., 1995. Kinetic analysis of the fate of nitric oxide synthesized by macrophages in vitro. J. Biol. Chem. 270 (49), 29350–29355.
Lim, C.H., Dedon, P.C., Deen, W.M., 2008. Kinetic analysis of intracellular concentrations of reactive nitrogen species. Chem. Res. Toxicol. 21 (11), 2134–2147.
Lyczak, J.B., Cannon, C.L., Pier, G.B., 2000. Establishment of Pseudomonas aeruginosa infection: lessons from a versatile opportunist. Microbes Infect. 2 (9), 1051–1060.
Mason, M.G., et al., 2009. Cytochrome *bd* confers nitric oxide resistance to *Escherichia coli*. Nat. Chem. Biol. 5 (2), 94–96.
Miller, C.C., et al., 2013. Inhaled nitric oxide decreases the bacterial load in a rat model of Pseudomonas aeruginosa pneumonia. J. Cyst. Fibros. 12 (6), 817–820.
Miller, L.C., et al., 2015. Development of potent inhibitors of pyocyanin production in Pseudomonas aeruginosa. J. Med. Chem. 58 (3), 1298–1306.
Nathan, C., 1992. Nitric-oxide as a secretory product of mammalian-cells. FASEB J. 6 (12), 3051–3064.
Oberhardt, M.A., Puchałka, J., Fryer, K.E., Martins dos Santos, V.A., Papin, J.A., 2008. Genome-scale metabolic network analysis of the opportunistic pathogen Pseudomonas aeruginosa PAO1. J. Bacteriol. 190 (8), 2790–2803.
Oberhardt, M.A., Goldberg, J.B., Hogardt, M., Papin, J.A., 2010. Metabolic network analysis of pseudomonas aeruginosa during chronic cystic fibrosis lung infection. J. Bacteriol. 192 (20), 5534–5548.
Oberhardt, M.A., Puchalka, J., Martins dos Santos, V.A., Papin, J.A., 2011. Reconciliation of genome-scale metabolic reconstructions for comparative systems analysis. PLoS Comput. Biol. 7 (3), e1001116.
O'Loughlin, C.T., et al., 2013. A quorum-sensing inhibitor blocks Pseudomonas aeruginosa virulence and biofilm formation. Proc. Natl. Acad. Sci. USA 110 (44), 17981–17986.
O'Toole, G.A., Kolter, R., 1998. Flagellar and twitching motility are necessary for

Pseudomonas aeruginosa biofilm development. Mol. Microbiol. 30 (2), 295–304.
Pacher, P., Beckman, J.S., Liaudet, L., 2007. Nitric oxide and peroxynitrite in health and disease. Physiol. Rev. 87 (1), 315–424.
Palmer, K.L., Brown, S.A., Whiteley, M., 2007. Membrane-bound nitrate reductase is required for anaerobic growth in cystic fibrosis sputum. J. Bacteriol. 189 (12), 4449–4455.
Platzen, L., Koch-Koerfges, A., Weil, B., Brocker, M., Bott, M., 2014. Role of flavohaemoprotein Hmp and nitrate reductase NarGHJI of Corynebacterium glutamicum for coping with nitrite and nitrosative stress. FEMS Microbiol. Lett. 350 (2), 239–248.
Poole, K., 2011. Pseudomonas aeruginosa: resistance to the max. Front. Microbiol. 2, 65.
Poole, R.K., Hughes, M.N., 2000. New functions for the ancient globin family: bacterial responses to nitric oxide and nitrosative stress. Mol. Microbiol. 36 (4), 775–783.
Rasko, D.A., Sperandio, V., 2010. Anti-virulence strategies to combat bacteria-mediated disease. Nat. Rev. Drug Discov. 9 (2), 117–128.
Reutov, V.P., Sorokina, E.G., 1998. NO-synthase and nitrite-reductase components of nitric oxide cycle. Biochemistry 63 (7), 874–884.
Robinson, J.L., Brynildsen, M.P., 2013. A kinetic platform to determine the fate of nitric oxide in Escherichia coli. PLoS Comput. Biol. 9 (5), e1003049.
Robinson, J.L., Brynildsen, M.P., 2015. An ensemble-guided approach identifies ClpP as a major regulator of transcript levels in nitric oxide-stressed Escherichia coli. Metab. Eng. 31, 22–34.
Robinson, J.L., Brynildsen, M.P., 2016a. Discovery and dissection of metabolic oscillations in the microaerobic nitric oxide response network of Escherichia coli. Proc. Natl. Acad. Sci. USA 113 (12), E1757–E1766.
Robinson, J.L., Brynildsen, M.P., 2016b. Construction and experimental validation of a quantitative kinetic model of nitric oxide stress in enterohemorrhagic *Escherichia coli* O157:H7. Bioengineering 3 (1).
Robinson, J.L., Adolfsen, K.J., Brynildsen, M.P., 2014a. Deciphering nitric oxide stress in bacteria with quantitative modeling. Curr. Opin. Microbiol. 19, 16–24.
Robinson, J.L., Miller, R.V., Brynildsen, M.P., 2014b. Model-driven identification of dosing regimens that maximize the antimicrobial activity of nitric oxide. Metab. Eng. Commun. 1, 12–18.
Romeo, A., et al., 2012. Transcriptional regulation of nitrate assimilation in Pseudomonas aeruginosa occurs via transcriptional antitermination within the nirBD-PA1779-cobA operon. Microbiol.-Sgm 158, 1543–1552.
Sasaki, Y., et al., 2016. Nitrogen oxide cycle regulates nitric oxide levels and bacterial cell signaling. Sci. Rep. 6, 22038.
Schreiber, K., et al., 2007. The anaerobic regulatory network required for Pseudomonas aeruginosa nitrate respiration. J. Bacteriol. 189 (11), 4310–4314.
Shapleigh, J.P., Davies, K.J.P., Payne, W.J., 1987. Detergent inhibition of nitric-oxide reductase-activity. Biochim. Biophys. Acta 911 (3), 334–340.
Shen, Y., Siryaporn, A., Lecuyer, S., Gitai, Z., Stone, H.A., 2012. Flow directs surface-attached bacteria to twitch upstream. Biophys. J. 103 (1), 146–151.
Silvestrini, M.C., Tordi, M.G., Musci, G., Brunori, M., 1990. The reaction of Pseudomonas nitrite reductase and nitrite. A stopped-flow and EPR study. J. Biol. Chem. 265 (20), 11783–11787.
Silvestrini, M.C., Falcinelli, S., Ciabatti, I., Cutruzzola, F., Brunori, M., 1994. Pseudomonas aeruginosa nitrite reductase (or cytochrome oxidase): an overview. Biochimie 76 (7), 641–654.
Siryaporn, A., Kuchma, S.L., O'Toole, G.A., Gitai, Z., 2014. Surface attachment induces Pseudomonas aeruginosa virulence. Proc. Natl. Acad. Sci. USA 111 (47), 16860–16865.
SooHoo, C.K., Hollocher, T.C., 1991. Purification and characterization of nitrous oxide reductase from Pseudomonas aeruginosa strain P2. J. Biol. Chem. 266 (4), 2203–2209.
Tsikas, D., 2007. Analysis of nitrite and nitrate in biological fluids by assays based on the Griess reaction: appraisal of the Griess reaction in the L-arginine/nitric oxide area of research. J. Chromatogr. B Anal. Technol. Biomed. Life Sci. 851 (1–2), 51–70.
Turkheimer, F.E., Hinz, R., Cunningham, V.J., 2003. On the undecidability among kinetic models: from model selection to model averaging. J. Cereb. Blood Flow. Metab. 23 (4), 490–498.
Van Alst, N.E., Picardo, K.F., Iglewski, B.H., Haidaris, C.G., 2007. Nitrate sensing and metabolism modulate motility, biofilm formation, and virulence in Pseudomonas aeruginosa. Infect. Immun. 75 (8), 3780–3790.
Van Alst, N.E., Wellington, M., Clark, V.L., Haidaris, C.G., Iglewski, B.H., 2009a. Nitrite reductase NirS is required for Type III secretion system expression and virulence in the human monocyte cell line THP-1 by Pseudomonas aeruginosa. Infect. Immun. 77 (10), 4446–4454.
Van Alst, N.E., Sherrill, L.A., Iglewski, B.H., Haidaris, C.G., 2009b. Compensatory periplasmic nitrate reductase activity supports anaerobic growth of Pseudomonas aeruginosa PAO1 in the absence of membrane nitrate reductase. Can. J. Microbiol. 55 (10), 1133–1144.
Varga, J.J., et al., 2015. Genotypic and phenotypic analyses of a Pseudomonas aeruginosa chronic bronchiectasis isolate reveal differences from cystic fibrosis and laboratory strains. BMC Genom. 16, 883.
Winsor, G.L., et al., 2016. Enhanced annotations and features for comparing thousands of Pseudomonas genomes in the Pseudomonas genome database. Nucleic Acids Res. 44 (D1), D646–653.
Winstanley, C., O'Brien, S., Brockhurst, M.A., 2016. Pseudomonas aeruginosa evolutionary adaptation and diversification in cystic fibrosis chronic lung infections. Trends Microbiol. 24 (5), 327–337.
Wolff, J.A., MacGregor, C.H., Eisenberg, R.C., Phibbs, P.V., Jr., 1991. Isolation and characterization of catabolite repression control mutants of Pseudomonas aeruginosa PAO. J. Bacteriol. 173 (15), 4700–4706.
Yoon, S.S., et al., 2002. Pseudomonas aeruginosa anaerobic respiration in biofilms: relationships to cystic fibrosis pathogenesis. Dev. Cell 3 (4), 593–603.
Yoon, S.S., et al., 2006. Anaerobic killing of mucoid Pseudomonas aeruginosa by acidified nitrite derivatives under cystic fibrosis airway conditions. J. Clin. Investig. 116 (2), 436–446.
Zamora-Sillero, E., Hafner, M., Ibig, A., Stelling, J., Wagner, A., 2011. Efficient characterization of high-dimensional parameter spaces for systems biology. BMC Syst. Biol. 5.
Zumft, W.G., 1997. Cell biology and molecular basis of denitrification. Microbiol. Mol. Biol. Rev. 61 (4), 533–616.